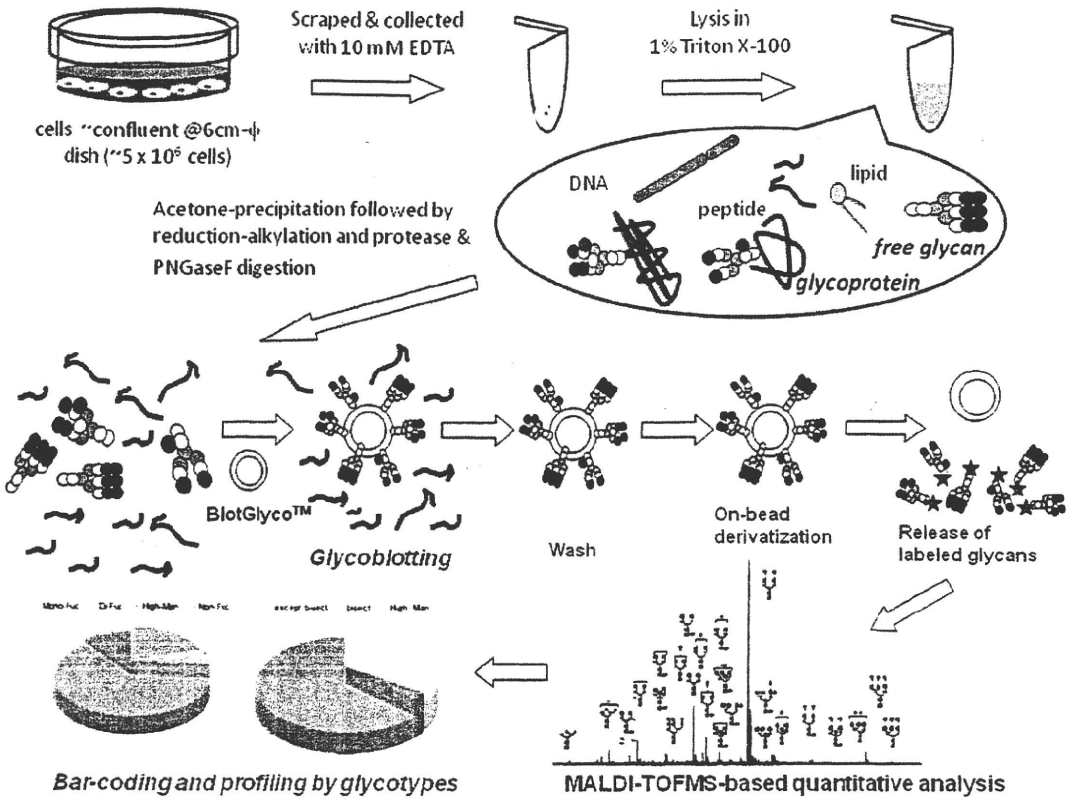

FIG. 1. **Basic protocol of high throughput and quantitative cellular glycomics based on glycoblotting method using BlotGlyco H bead.** ϕ, inner diameter; *PNGaseF*, peptide-*N*-glycosidase F.

beads via stable hydrazone bonds. The plate was washed by 200 μl of 2 M guanidine HCl in ammonium bicarbonate followed by washing with the same volume of water and 1% triethylamine in methanol (MeOH). Each washing step was performed twice, respectively. Unreacted hydrazide functional groups on beads were capped by incubation with 10% acetic anhydride in MeOH for 30 min at room temperature. Then the solution was removed by vacuum, and then the bead was serially washed by 2 × 200 μl of 10 mM HCl, MeOH, and dioxane, respectively. On-bead methyl esterification of carboxyl groups in sialic acids was carried out by incubation with 150 mM 3-methyl-1-*p*-tolyltriazene in dioxane at 60 °C to dryness. It usually took 90 min in a conventional oven. Then the bead was serially washed by 200 μl of dioxane, water, MeOH, and water. The glycans blotted on beads were subjected to the *trans*-iminization reaction with aoWR (aminooxy-functionalized peptide reagent) for 45 min at 80 °C. WR-tagged glycans were eluted by adding 100 μl of water and then purified by a Mass PREP™ hydrophilic interaction chromatography (HILIC) μElution Plate (Waters) according to the manufacturer's description.

The purified *N*-glycans were 10-fold concentrated by SpeedVac followed by direct dissolution with 2,5-dihydroxylbenzoic acid (10 mg/ml in 30% ACN) and were crystallized. Then the analytes were subjected to MALDI-TOF-MS analysis using an Ultraflex time-of-flight mass spectrometer III (Bruker Daltonics, Billerica, MA) in reflector, positive ion mode typically summing 1000 shots. The detected *N*-glycan peaks in MALDI-TOF-MS spectra were picked using the software FlexAnalysis version 3 (Bruker Daltonics) in independently performed experiments in P19C6, P19CL6, and ESCs, respectively. The intensity of the isotopic peaks of each glycan was normalized to 15 pmol of internal standard (A2 amide glycan) in each status. The changes of glycan expression levels were calculated as differentiated *versus* undifferentiated. Student's *t* test was used to calculate the statistical difference of cell status, namely differentiated *versus* undifferentiated. The glycan structures were speculated using GlycoMod Tool and GlycoSuite.

RT-PCR—RNA was extracted from 1.5–5 × 10^7 P19CL6 cells using an "R&D Quick" kit (Dainippon Sumitomo Pharma Co., Ltd., Osaka, Japan) according to the manufacturer's instructions. RT-PCR was performed using the SuperScriptIII One-Step RT-PCR System with Platinum *Taq* DNA polymerase (Invitrogen) to reverse transcribe and amplify cDNAs coding the proteins described below. The primer sequences were as follows: β-actin, 3′-TGTGATGGTGGGAATGGGTCGG-5′ and 5′-TTTGATGTCACGCACGATTTCC-3′; α-cardiac myosin heavy chain, 3′-CTGCTGGAGAGGTTATTCCTCG-5′ and 5′-GGAAGAGTGAGCGGCGCATCAAGG-3′; and β-cardiac myosin heavy chain, 3′-TGCAAAGGCTCCAGGTCTGAGGGC-5′ and 5′-GCCAACACCAACCTGTCCAAGTTC-3′).

Immunohistochemistry—Sixteen days after incubation with or without 1% DMSO, P19CL6 cells were collected as described above and dissociated intensively by EDTA/PBS containing 0.05% trypsin. After washing, cells were dissolved in PBS and smeared onto silane-coated slide glass (SUPERFROST®, Matsunami Glass, Osaka, Japan). Cells were fixed in cold acetone and treated with MeOH containing 3% H_2O_2 for 10 min at room temperature to quench internal peroxidase activity. Nonspecific binding on cells was blocked by incubation with CAS-Block (Zymed Laboratories Inc.) for 10 min at room temperature. Cells were then incubated with MF20 (1:800) (The monoclonal antibody developed by Donald A. Fischman was obtained from the Developmental Studies Hybridoma Bank developed under the auspices of the NICHD, National Institutes of Health and maintained by The University

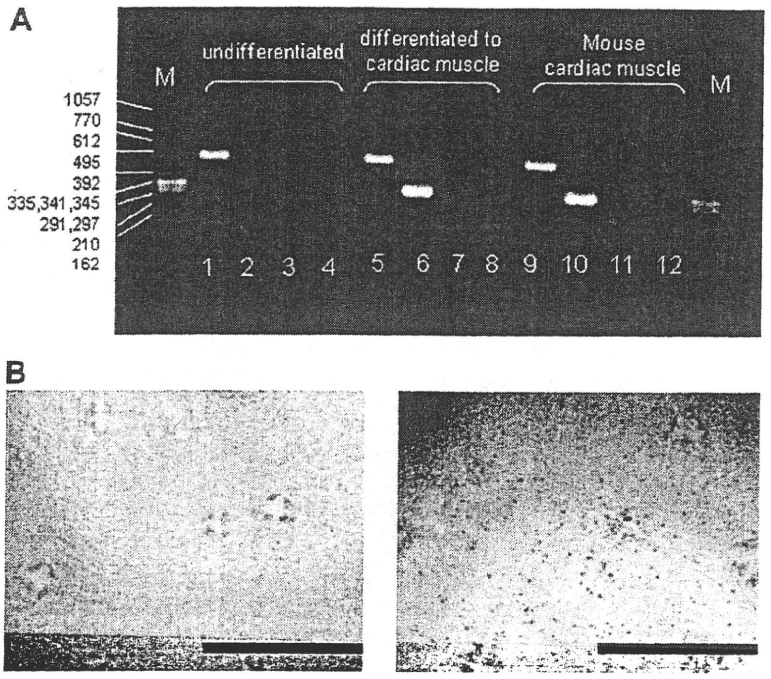

FIG. 2. **Differentiation of P19CL6 cells to cardiomyocytes in presence of DMSO.** *A*, RT-PCR analysis for the confirmation of cellular differentiation to cardiac muscle. *M*, DNA size marker (bp); *lanes 1*, *5*, and *9*, β-actin (503 bp), *lanes 2*, *6*, and *10*, α-cardiac myosin heavy chain (302 bp); *lanes 3*, *7*, and *11*, β-cardiac myosin heavy chain (205 bp); *lanes 4*, *8*, and *12*, embryonic skeletal muscle (151 bp). *B*, immunocytochemistry for the confirmation of P19CL6 cell differentiation to cardiac muscle. Primary antibody, MF20 (mouse monoclonal anti-sarcomere myosin); secondary antibody, HRP polymer-conjugated IgG; chromogenic substrate, diaminobenzidine. The *bar* represents 1.0 cm.

of Iowa, Department of Biological Sciences, Iowa City, IA.), which is a sarcomeric myosin-specific monoclonal antibody, overnight at 4 °C. They were then washed by PBS and incubated with HRP-labeled secondary antibody (Zymed Laboratories Inc.) for 10 min at room temperature. After washing, diaminobenzidine solution was added, and the reaction was stopped by washing with water. In the case of P19C6, anti-mouse neurofilament 160 was used as the primary antibody, and the other part of the procedure was performed similarly.

RESULTS

Concept—Our strategy of a glycoblotting-based rapid and quantitative glycomics designed for whole cellular *N*-glycans/free oligosaccharides using BlotGlyco (BlotGlyco H) beads is diagrammed in Fig. 1. The specific steps of this optimized protocol involve (i) enzymatic release of entire *N*-glycans from cellular glycoprotein fractions, including both cell surface and endogenous glycoproteins, (ii) glycoblotting (chemoselective enrichment) by BlotGlyco beads, (iii) on-bead derivatization and labeling with a reagent to enhance MS sensitivity by *trans*-iminization, and (iv) subsequent quantitative mass spectrometry-based glycomics and typing subgroups of characteristic glycoforms, namely glycotypes, in the presence of an internal standard. The key difference when compared with other published approaches for cellular glycomics is specific chemistry-based enrichment of entire *N*-glycans by a commercially available high density hydrazide bead (BlotGlyco) that allows for high throughput and quantitative glycan profiling. Through on-bead chemical protection of carboxyl groups, both human sialic acid Neu5Ac and non-human sialic acid Neu5Gc are stabilized to prevent the significant cleavage at the sensitive *O*-glycoside linkage of sialosides during the high energy ionization process in mass spectrometry. Given that human ESCs and iPS cells currently being developed are produced by using animal-derived materials such as serum and feeder layers or even fractionated glycoproteins, it is important to address potential contamination by introduction of non-human sialic acid Neu5Gc into human stem cell lines proposed for therapeutic applications in humans (13, 21). The reaction conditions and all procedures are carefully optimized by using not only mouse embryonic cells but also various human cancer cell lines to maximize efficacy of *N*-glycan enrichment and reproducibility of data acquisition. To facilitate quantitative *N*-glycan profiling analysis, the expression level of individual *N*-glycans was normalized and represented by using a standardized unit (pmol/200 μg of cellular proteins). We note that the present protocol is readily feasible for any type of mammalian cells, and the efficiency of glycoblotting is not dependent on cell type when the required cell numbers (for example, confluence on a 6-cm dish; ~5 × 10^6 cells) can be prepared. Rapid and quantitative analysis of major *N*-glycans (60–80 major glycoforms) enriched by the glycoblotting method provided us with reliable and satisfactory information for investigating structural changes in entire *N*-glycans and comparing the ratio of significant glycoforms by bar coding with characteristic subtypes, namely stage-specific embryonic glycotypes, during dynamic cell differentiation and proliferation.

Monitoring Entire N-Glycan Expression during Mouse P19 Cell Differentiations—Herein we selected the mouse P19 subclone to evaluate efficiency and versatility of our glycoblotting-based strategy. P19C6 cells are mouse embryonic car-

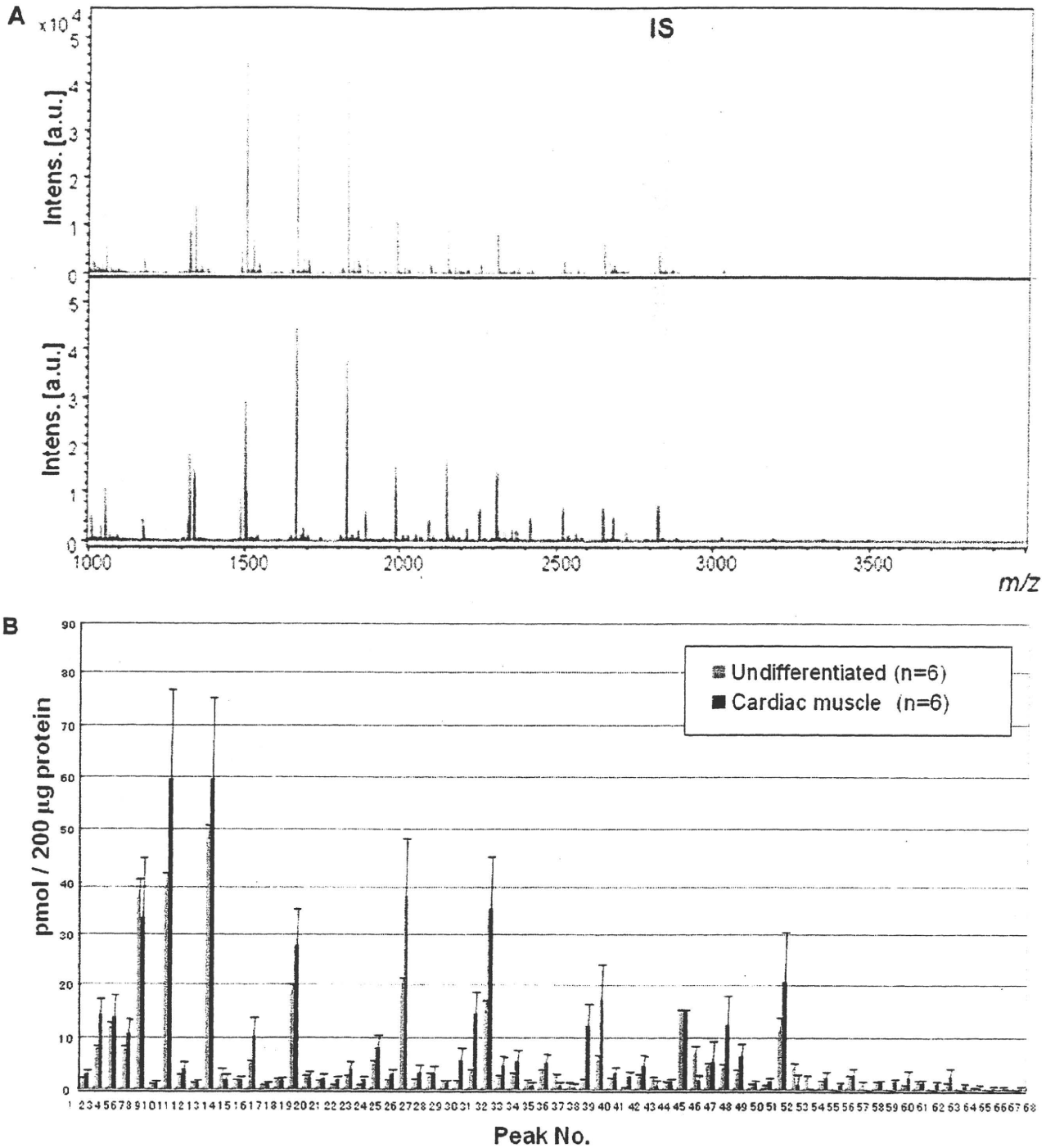

FIG. 3. **Large scale *N*-glycan analysis during P19CL6 cell differentiation.** *A*, MALDI-TOF-MS of whole *N*-glycans of undifferentiated and differentiated cells. *IS*, internal standard. *B*, quantitative and total glycomics of undifferentiated and differentiated cells. *C*, magnification to visualize increased glycans (*, $p < 0.01$; **, $p < 0.05$). *D*, magnification to visualize decreased glycans (*, $p < 0.01$; **, $p < 0.05$). Error bars mean standard deviations. *E*, bar coding analysis. *Intens.*, intensity; *a.u.*, arbitrary units.

cinoma cells and serve as a common model for studying neuronal differentiation after RA inducement (32). P19 cells treated with lower level RA or DMSO differentiate into muscle (33), and P19CL6 cells, a well established subclone derived from P19 cells, efficiently differentiate into beating cardiomyocytes by treatment with 1% DMSO (27, 34).

Differentiation of P19CL6 Cells to Cardiomyocytes—In the present study, we carefully characterized whole *N*-glycans of

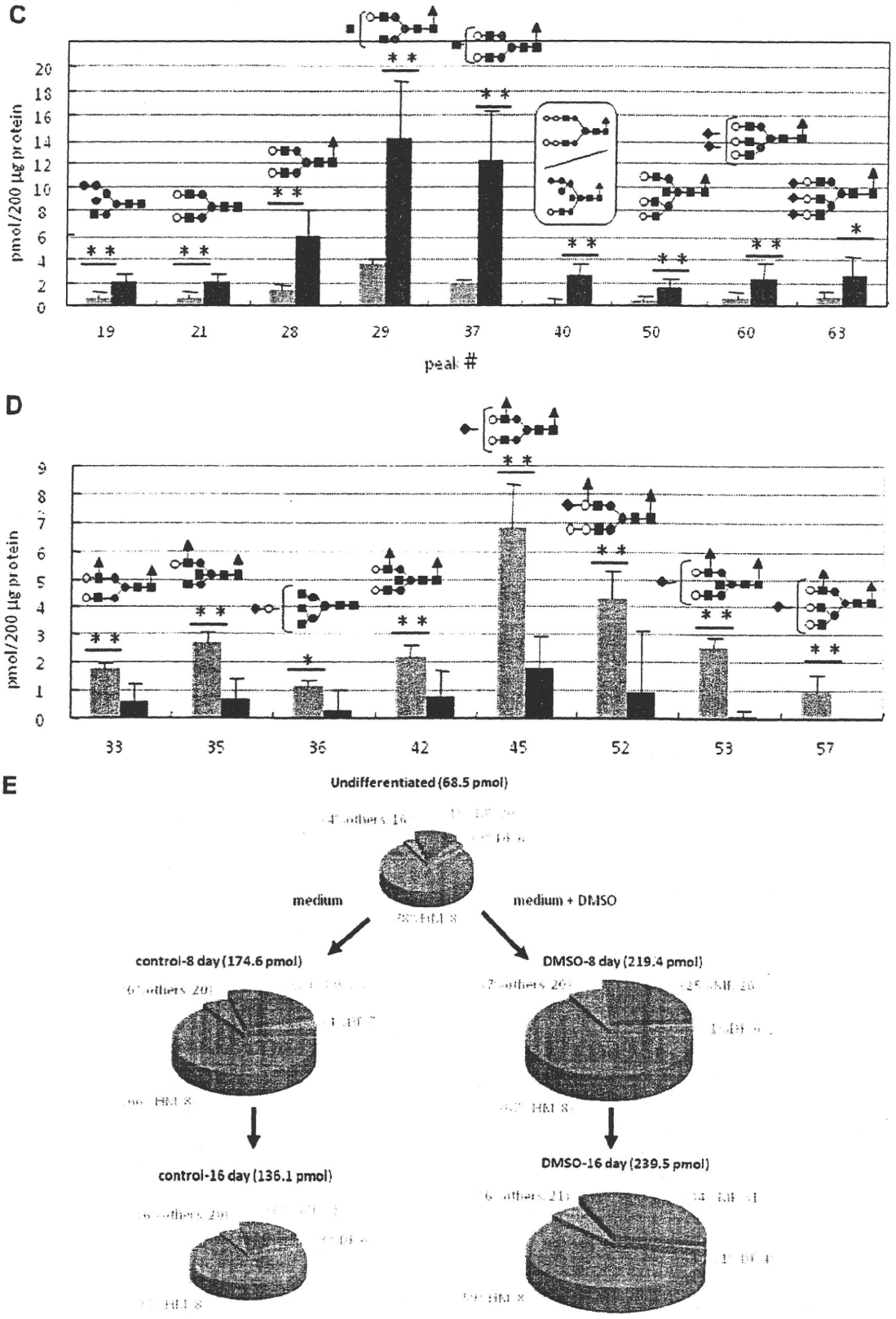

FIG. 3—*continued*

TABLE I
Glycoforms detected during P19CL6 cell differentiation
Hex, hexose; dHex, deoxyhexose; HexNAc, *N*-acetylhexosamine.

Peak no. CL6	*m/z*	Composition
1	1178.50	$Hex_2(HexNAc)_2$
2	1324.55	$Hex_2(HexNAc)_2dHex_1$
3	1340.55	$Hex_3(HexNAc)_2$
4	1486.61	$Hex_3(HexNAc)_2dHex_1$
5	1502.60	$Hex_4(HexNAc)_2$
6	1543.63	$Hex_3(HexNAc)_3$
7	1664.65	$Hex_5(HexNAc)_2$
8	1689.69	$Hex_3(HexNAc)_3dHex_1$
9	1746.71	$Hex_3(HexNAc)_4$
10	1826.71	$Hex_6(HexNAc)_2$
11	1848.74	$Hex_3(HexNAc)_4(NeuAc)_1$
12	1851.74	$Hex_4(HexNAc)_3dHex_1$
13	1892.76	$Hex_3(HexNAc)_4dHex_1$
14	1908.76	$Hex_4(HexNAc)_4$
15	1949.79	$Hex_3(HexNAc)_5$
16	1988.76	$Hex_7(HexNAc)_2$
17	2010.79	$Hex_4(HexNAc)_3(NeuAc)_1$
18	2013.79	$Hex_5(HexNAc)_3dHex_1$
19	2029.79	$Hex_6(HexNAc)_3(NeuAc)_1$
20	2054.82	$Hex_4(HexNAc)_4dHex_1$
21	2070.81	$Hex_5(HexNAc)_4$
22	2095.84	$Hex_3(HexNAc)_5dHex_1$
23	2111.84	$Hex_4(HexNAc)_5$
24	2150.81	$Hex_8(HexNAc)_2$
25	2156.85	$Hex_4(HexNAc)_3dHex_1(NeuAc)_1$
26	2172.84	$Hex_5(HexNAc)_3(NeuAc)_1$
27	2213.87	$Hex_4(HexNAc)_4(NeuAc)_1$
28	2216.87	$Hex_5(HexNAc)_4dHex_1$
29	2257.90	$Hex_4(HexNAc)_5dHex_1$
30	2312.86	$Hex_9(HexNAc)_2$
31	2334.90	$Hex_6(HexNAc)_3(NeuAc)_1$
32	2359.93	$Hex_4(HexNAc)_4dHex1(NeuAc)_1$
33	2362.93	$Hex_5(HexNAc)_4dHex_2$
34	2375.92	$Hex_5(HexNAc)_4(NeuAc)_1$
35	2403.95	$Hex_4(HexNAc)_5dHex_2$
36	2416.95	$Hex_4(HexNAc)_6(NeuAc)_1$
37	2419.95	$Hex_5(HexNAc)_5dHex_1$
38	2521.98	$Hex_5(HexNAc)_4dHex_1(NeuAc)_1$
39	2537.98	$Hex_6(HexNAc)_4(NeuAc)_1$
40	2540.98	$Hex_7(HexNAc)_5dHex_1$
41	2563.01	$Hex_4(HexNAc)_5dHex_1(NeuAc)_1$
42	2566.01	$Hex_5(HexNAc)_5dHex_2$
43	2579.00	$Hex_5(HexNAc)_5(NeuAc)_1$
44	2651.33	Internal standard
45	2668.04	$Hex_5(HexNAc)_4dHex_2(NeuAc)_1$
46	2681.03	$Hex_5(HexNAc)_4(NeuAc)_2$
47	2684.03	$Hex_6(HexNAc)_4dHex_1(NeuAc)_1$
48	2725.06	$Hex_5(HexNAc)_5dHex_1(NeuAc)_1$
49	2741.06	$Hex_6(HexNAc)_6(NeuAc)_1$
50	2785.08	$Hex_6(HexNAc)_6dHex_1$
51	2827.09	$Hex_5(HexNAc)_4dHex_1(NeuAc)_2$
52	2830.09	$Hex_6(HexNAc)_4dHex_2(NeuAc)_1$
53	2871.12	$Hex_5(HexNAc)_5dHex_2(NeuAc)_1$
54	2887.11	$Hex_6(HexNAc)_5dHex_1(NeuAc)_1$
55	2928.14	$Hex_5(HexNAc)_6dHex_1(NeuAc)_1$
56	3030.17	$Hex_5(HexNAc)_5dHex_1(NeuAc)_2$
57	3033.17	$Hex_6(HexNAc)_5dHex_2(NeuAc)_1$
58	3046.17	$Hex_6(HexNAc)_5(NeuAc)_2$
59	3090.19	$Hex_6(HexNAc)_5dHex_1(NeuAc)_1$
60	3192.22	$Hex_6(HexNAc)_5dHex_1(NeuAc)_2$
61	3351.28	$Hex_6(HexNAc)_5(NeuAc)_3$
62	3395.30	$Hex_6(HexNAc)_6dHex_1(NeuAc)_2$
63	3497.34	$Hex_6(HexNAc)_5dHex_1(NeuAc)_3$
64	3557.36	$Hex_7(HexNAc)_6dHex_1(NeuAc)_2$
65	3700.42	$Hex_6(HexNAc)_6dHex_1(NeuAc)_3$
66	3862.47	$Hex_7(HexNAc)_6dHex_1(NeuAc)_3$
67	4021.52	$Hex_7(HexNAc)_6(NeuAc)_4$
68	4167.58	$Hex_7(HexNAc)_6dHex_1(NeuAc)_4$

P19C6 cells with or without inducement into neural cells as well P19CL6 cells differentiated into cardiomyocytes. After 1% DMSO treatment, P19CL6 cells formed a monolayer at day 3 and multilayers on day 5 and started beating synchronously at day 16 of differentiation as reported (27), whereas control cells did not show any changes at the same period of culture. The differentiation into cardiac muscle was confirmed by conventional RT-PCR detecting mRNA coding cardiomyocyte-specific proteins and immunocytochemistry (Fig. 2, *A* and *B*). As shown in Fig. 2*A*, α- and β-cardiac myosin heavy chains, the markers of cardiomyocytes (35), were specifically detected in the DMSO-treated 16-day cultured P16CL6 cells and mouse cardiac muscles as a positive control. In addition, mouse monoclonal antibody MF20 reacted specifically with differentiated cardiomyocytes (Fig. 2*B*), indicating that differentiated cells readily express sarcomeric myosin.

Whole *N*-glycans of P19CL6 cells (undifferentiated cells) and differentiated cells on day 18 ($n = 6$, six dishes each for both cells) were analyzed and identified for the first time by means of glycoblotting-based high throughput MALDI-TOF mass spectrometry (Fig. 3*A*). As summarized in Table I, 67 kinds of glycoforms were detected and quantified reproducibly in both cases. When the full portraits of *N*-glycan diversity of both cells were represented quantitatively (Fig. 3*B*), it seems likely that high mannose type *N*-glycans (peak numbers 1(M2), 3(M3), 5(M4), 7(M5), 10(M6), 16(M7), 24(M8), and 30(M9)) are major components throughout cardiomyocytic differentiation. However, it was also clearly suggested that expression levels of 26 *N*-glycans were significantly accompanied by cellular differentiation; 19 *N*-glycans, most of which are monofucosylated glycoforms, were increased concertedly, whereas seven difucosylated *N*-glycans decreased. Changes in two glycoforms (peak numbers 40 and 53) were especially significant ($p < 0.001$); their expression level was increased 16-fold (peak number 40) and decreased 30-fold (peak number 53) according to differentiation, respectively. Fig. 3, *C* and *D*, highlights dramatically changed *N*-glycan structures during cell differentiation; namely monofucosylated *N*-glycans were drastically increased, whereas difucosylated *N*-glycans decreased in comparison with the expression level of whole cellular *N*-glycans.

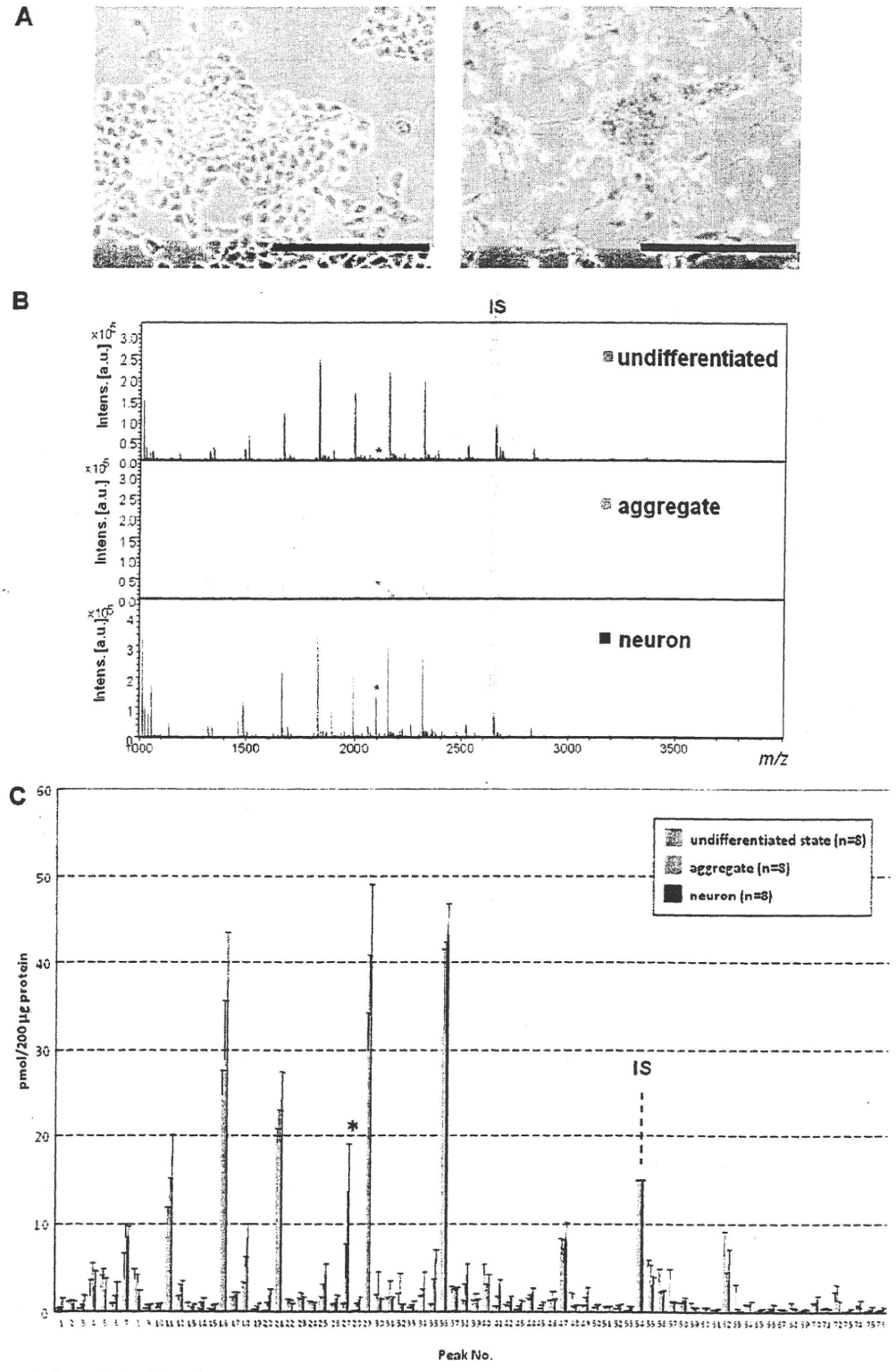

FIG. 4. **Differentiation of P19C6 cells to neural cells.** *A*, immunocytochemistry for the confirmation of neural differentiation. Primary antibody, mouse monoclonal anti-neurofilament 160; secondary antibody, HRP polymer-conjugated IgG; chromogenic substrate, diaminobenzidine. The *bar* represents 200 μm. *B*, MALDI-TOF-MS of whole *N*-glycans of undifferentiated and differentiated cells. *IS*, internal standard. * represents peak number 27. *C*, quantitative and total glycomics of undifferentiated and differentiated cells. *IS*, internal standard. * represents peak number 27. *D*, magnification to visualize increased glycans. *E*, bar coding analysis.

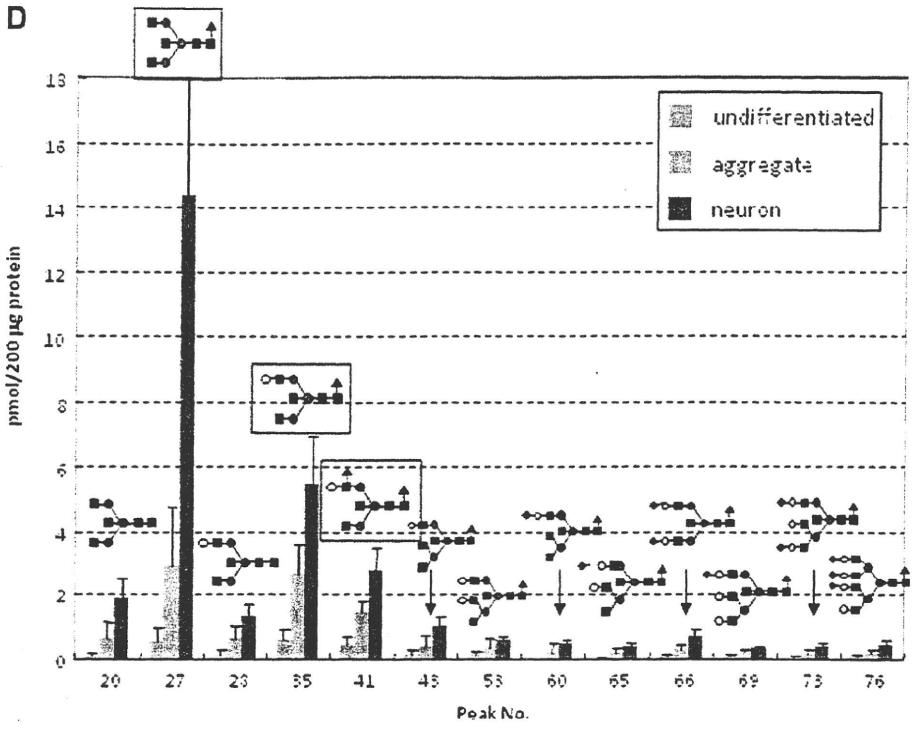

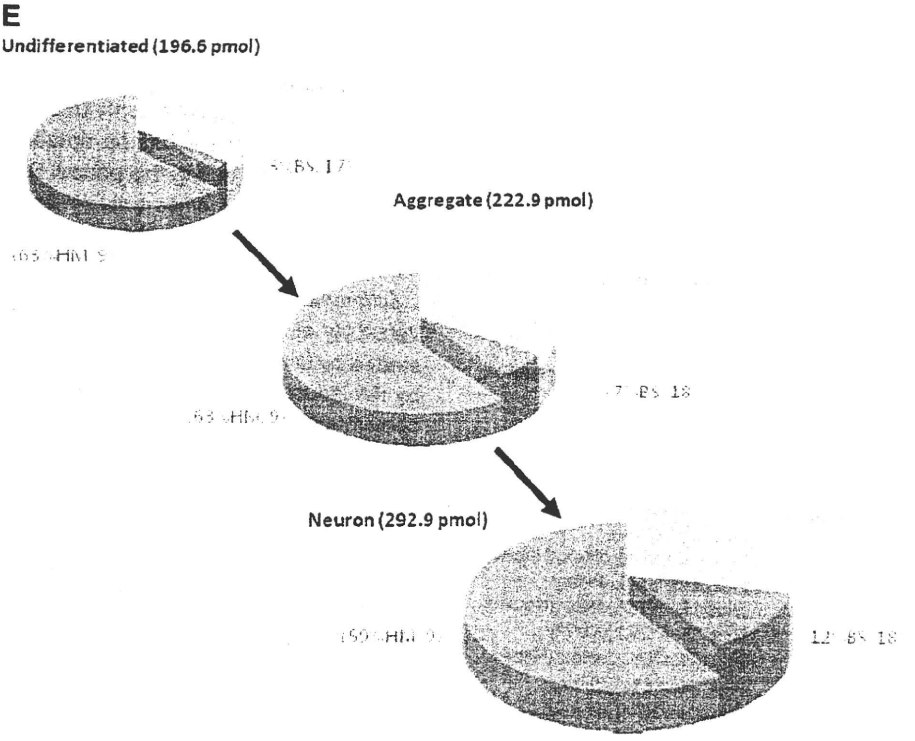

FIG. 4—*continued*

The significance of the dramatic changes in the expression level of two distinct glycotypes uncovered by quantitative glycomics of entire cellular *N*-glycans was revealed much more simply by bar coding individual glycotypes such as high mannose type (HM), monofucosylated type (MF), difucosylated type (DF), and others (O) (Fig. 3*E*). It is clear that the total *N*-glycan expression level was significantly increased from undifferentiated (68.5 pmol/200 μg of protein) to the interme-

TABLE II
Glycoforms detected during P19C6 cell differentiation
Hex, hexose; dHex, deoxyhexose; HexNAc, *N*-acetylhexosamine.

Peak no.	*m/z*	Composition
1	1137.47	$Hex_3(HexNAc)_1$
2	1178.50	$Hex_2(HexNAc)_2$
3	1299.52	$Hex_4(HexNAc)_1$
4	1324.55	$Hex_2(HexNAc)_2dHex_1$
5	1340.55	$Hex_3(HexNAc)_2$
6	1461.57	$Hex_5(HexNAc)_1$
7	1486.61	$Hex_3(HexNAc)_2dHex_1$
8	1502.60	$Hex_4(HexNAc)_2$
9	1543.63	$Hex_3(HexNAc)_3$
10	1623.63	$Hex_6(HexNAc)_1$
11	1664.65	$Hex_5(HexNAc)_2$
12	1689.69	$Hex_3(HexNAc)_3dHex_1$
13	1705.68	$Hex_4(HexNAc)_3$
14	1746.71	$Hex_3(HexNAc)_4$
15	1785.68	$Hex_7(HexNAc)_1$
16	1826.71	$Hex_6(HexNAc)_2$
17	1851.74	$Hex_4(HexNAc)_3dHex_1$
18	1892.76	$Hex_3(HexNAc)_4dHex_1$
19	1908.76	$Hex_4(HexNAc)_4$
20	1949.79	$Hex_3(HexNAc)_5$
21	1988.76	$Hex_7(HexNAc)_2$
22	2010.79	$Hex_4(HexNAc)_3(NeuAc)_1$
23	2013.79	$Hex_5(HexNAc)_3dHex_1$
24	2029.79	$Hex_6(HexNAc)_3(NeuAc)_1$
25	2054.82	$Hex_4(HexNAc)_4dHex_1$
26	2070.81	$Hex_5(HexNAc)_4$
27	2095.84	$Hex_3(HexNAc)_5dHex_1$
28	2111.84	$Hex_4(HexNAc)_5$
29	2150.81	$Hex_6(HexNAc)_2$
30	2172.84	$Hex_5(HexNAc)_3(NeuAc)_1$
31	2175.84	$Hex_6(HexNAc)_3dHex_1$
32	2200.88	$Hex_4(HexNAc)_4dHex_2$
33	2213.87	$Hex_4(HexNAc)_4(NeuAc)_1$
34	2216.87	$Hex_5(HexNAc)_4dHex_1$
35	2257.90	$Hex_4(HexNAc)_5dHex_1$
36	2312.86	$Hex_9(HexNAc)_2$
37	2334.90	$Hex_6(HexNAc)_3(NeuAc)_1$
38	2359.93	$Hex_4(HexNAc)_4dHex_1(NeuAc)_1$
39	2362.93	$Hex_5(HexNAc)_4dHex_2$
40	2375.92	$Hex_5(HexNAc)_4(NeuAc)_1$
41	2403.95	$Hex_4(HexNAc)_5dHex_2$
42	2419.95	$Hex_5(HexNAc)_5dHex_1$
43	2460.98	$Hex_4(HexNAc)_6dHex_1$
44	2474.92	$Hex_{10}(HexNAc)_2$
45	2480.95	$Hex_6(HexNAc)_3dHex_1(NeuAc)_1$
46	2508.99	$Hex_5(HexNAc)_4dHex_3$
47	2521.98	$Hex_5(HexNAc)_4dHex_1(NeuAc)_1$
48	2537.98	$Hex_6(HexNAc)_4(NeuAc)_1$
49	2563.01	$Hex_4(HexNAc)_5dHex_1(NeuAc)_1$
50	2566.01	$Hex_5(HexNAc)_5dHex_2$
51	2579.00	$Hex_5(HexNAc)_5(NeuAc)_1$
52	2582.00	$Hex_6(HexNAc)_5dHex_1$
53	2623.03	$Hex_5(HexNAc)_6dHex_1$
54	2651.33	Internal standard
55	2668.04	$Hex_5(HexNAc)_4dHex_2(NeuAc)_1$
56	2681.03	$Hex_5(HexNAc)_4(NeuAc)_2$
57	2684.03	$Hex_6(HexNAc)_4dHex_1(NeuAc)_1$
58	2725.06	$Hex_5(HexNAc)_5dHex_1(NeuAc)_1$
59	2741.06	$Hex_6(HexNAc)_6(NeuAc)_1$
60	2766.09	$Hex_4(HexNAc)_6dHex_1(NeuAc)_1$
61	2785.08	$Hex_6(HexNAc)_6dHex_1$
62	2827.09	$Hex_5(HexNAc)_4dHex_1(NeuAc)_2$
63	2830.09	$Hex_6(HexNAc)_4dHex_2(NeuAc)_1$
64	2887.11	$Hex_6(HexNAc)_5dHex_1(NeuAc)_1$
65	2928.14	$Hex_5(HexNAc)_6dHex_1(NeuAc)_1$
66	3030.17	$Hex_5(HexNAc)_5dHex_1(NeuAc)_2$
67	3033.17	$Hex_6(HexNAc)_5dHex_2(NeuAc)_1$
68	3046.17	$Hex_6(HexNAc)_5(NeuAc)_2$
69	3090.19	$Hex_6(HexNAc)_6dHex_1(NeuAc)_1$
70	3192.22	$Hex_6(HexNAc)_5dHex_1(NeuAc)_2$
71	3338.28	$Hex_6(HexNAc)_5dHex2(NeuAc)_2$
72	3351.28	$Hex_6(HexNAc)_5(NeuAc)_3$
73	3395.30	$Hex_6(HexNAc)_6dHex_1(NeuAc)_2$
74	3497.34	$Hex_6(HexNAc)_5dHex_1(NeuAc)_3$
75	3557.36	$Hex_7(HexNAc)_6dHex_1(NeuAc)_2$
76	3862.47	$Hex_7(HexNAc)_6dHex_1(NeuAc)_3$

diate cells at day 8 (219.4 pmol/200 μg of protein) and differentiated cells at day 16 (239.5 pmol/200 μg of protein). It was revealed that the ratio of glycotype MF was increased from 15 to 34%, and at least 11 glycoforms could be assigned as newly generated *N*-glycans involved in the glycotype MF after differentiation, whereas the others, glycotype HM, glycotype DF, and glycotype O, showed no significant change both in the ratio and the number of glycoforms. When P19CL6 cells were subjected to culture continuously until day 16 without DMSO induction, there was no notable change in entire *N*-glycan expression during this period. Surprisingly, these cells exhibited *N*-glycan profiles quite similar to each other in terms of not only the ratio of the above four glycotypes but also the numbers of glycoforms identified in the individual glycotypes.

Differentiation of P19C6 Cells and ESCs to Neural Cells—Versatility of the present concept and protocol was demonstrated by using P19C6 cells that differentiate into neural cells by RA inducement in which differentiation can be confirmed conventionally by immunocytochemistry using mouse monoclonal antibody (anti-neurofilament 160 monoclonal antibody) as shown in Fig. 4*A*. Fig. 4*B* shows MALDI-TOF mass spectra of whole *N*-glycans enriched by glycoblotting at three distinct stages observed during P19C6 cell differentiation to neural cells, namely undifferentiated, aggregate (day 4), and differentiated neural cells (day 9). A total of 75 *N*-glycans were identified; they are summarized in Table II and represented in a quantitative manner in Fig. 4*C*. In the case of P19C6 cell differentiation into neural cells, it was revealed that 12 glycoforms (peak numbers 20, 27, 28, 35, 41, 43, 53, 60, 65, 66, 69, and 73) were identified as bisect type (BS) *N*-glycans among 13 *N*-glycans that increased more than 5-fold after differentiation (Fig. 4*D*). The merit of bar coding analysis based on the characteristic subtypes is clear because profiling by focusing on glycotype BS clearly shows a drastic increase of this subtype (from 3 to 12%) compared with glycotype HM (from

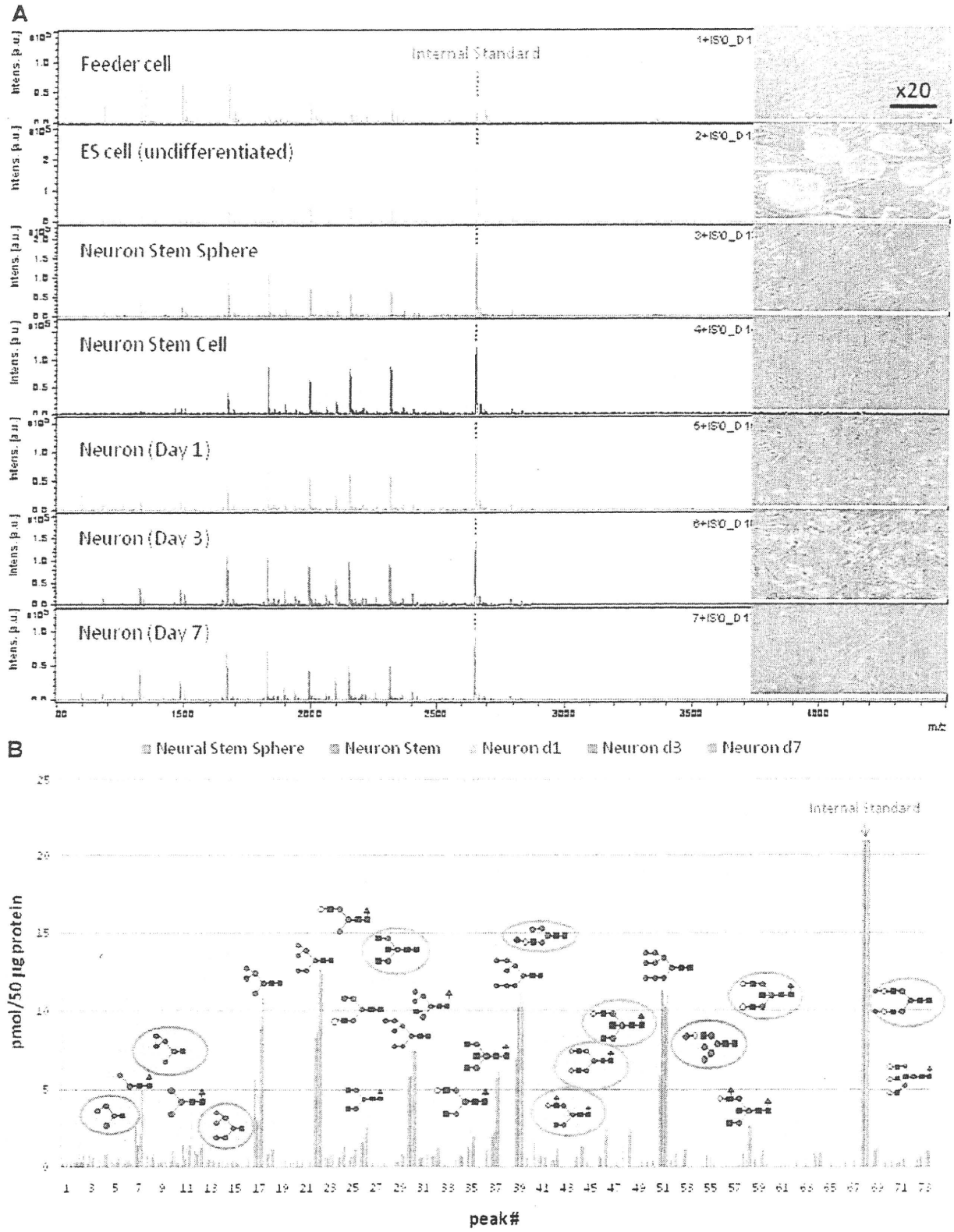

FIG. 5. **Differentiation of mouse ESCs to neural cells.** *A*, MALDI-TOF-MS spectra during cell differentiation. *B*, quantitative glycan profiling during ESC differentiation. *C*, bar coding analysis. *D*, novel glycan biomarkers for identifying and monitoring the processes of mouse neural cell differentiation. *Intens.*, intensity; *a.u.*, arbitrary units; *d*, day.

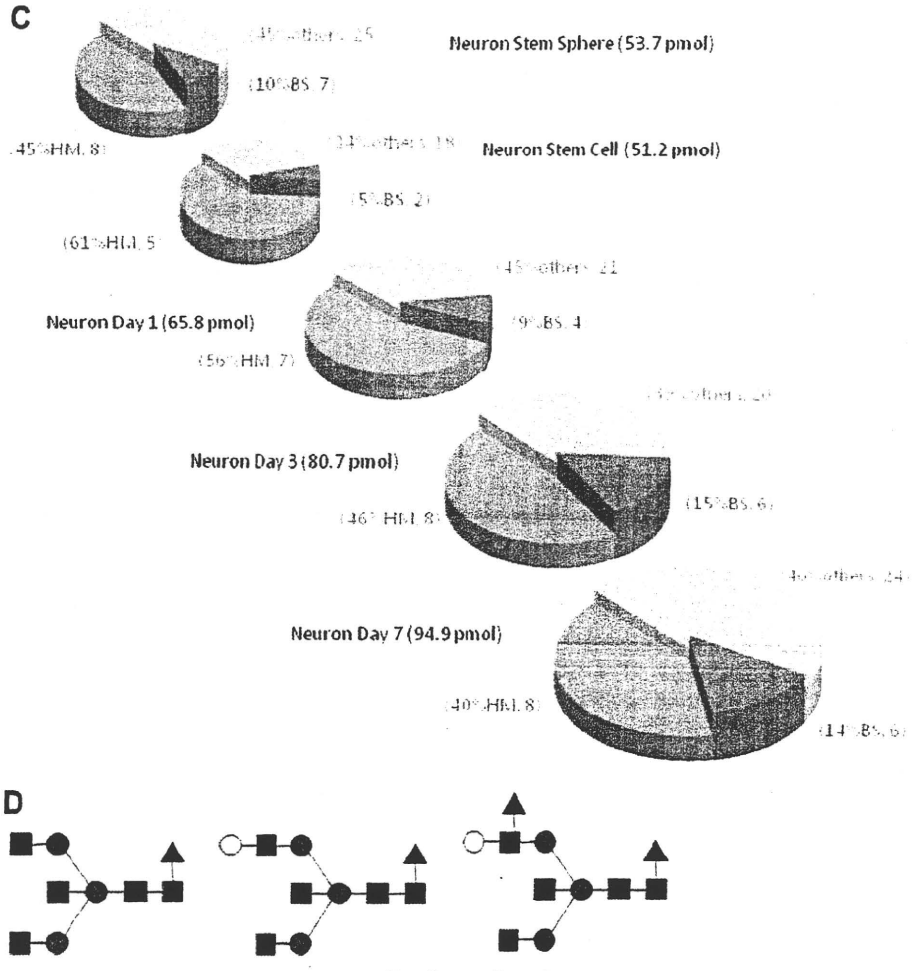

FIG. 5—*continued*

63 to 59%) and glycotype O (from 34 to 29%) (Fig. 4*E*). On the contrary, L-fucose-focused bar coding analysis used in the case of the P19CL6/cardiomyocytes system did not show any meaningful *N*-glycans expression change during differentiation: glycotype HM, from 63 to 59%; glycotype DF, from 6 to 4%; glycotype MF, from 21 to 30%; and glycotype O, from 10 to 7%.

Our interest was next directed toward alteration of *N*-glycan expression of mouse ESC differentiation to neural cells. We considered that neural cells differentiated from mouse ESCs should also exhibit a structural alteration in the stage-specific glycotypes, an increase of glycotype BS, similar to those observed in P19C6 cell differentiation. Fig. 5, *A* and *B*, and Table III show the results of MALDI-TOF-MS of all typical cellular stages during mouse ESC differentiation into neural cells. As expected, bar coding analysis by three glycotypes used in the P19C6 cells demonstrated the significant increase of glycotype BS (10% at neural stem sphere or 5% at neural stem cell to 14% at neural cell day 7) in comparison with glycotype HM (45% at neural stem sphere or 61% at neural stem cell to 40%) and glycotype O (45% at neural stem sphere or 34% at neural stem cell to 46%) (Fig. 5*C*). During the differentiation from neural stem sphere into neural stem cells, it seems likely that an increase of glycotype HM (from 45 to 61%) and a decrease of glycotype BS (from 10 to 5%) occurred concurrently, although the reason is not clear. Surprisingly, it was revealed that neural cells differentiated from ESCs also exhibited up-regulated high level expression of the same three glycoforms (Fig. 5*D*; peak numbers 37, 48, and 58 in Fig. 5*B*) as those observed in P19C6 differentiation (peak numbers 27, 35, and 41 in Fig. 4*D*). We could not detect any Neu5Gc residue in whole *N*-glycans identified in the present study, and the expression levels of any *N*-glycans containing Neu5Ac residue(s) did not accompany P19 series cell differentiation. This means that bar coding analysis focusing on the expression level of Neu5Ac did not work for identifying stage-specific embryonic glycotypes in these cell lines. Our preliminary result (n = 3) indicates clearly the importance of the stage-specific embryonic glycotype BS as a new class of biomarkers for identifying and monitoring processes of mouse ESC differentiation into neural cells, although the effect of feeder cells and other various factors

TABLE III
Glycoforms detected during ESC differentiation
Hex, hexose; dHex, deoxyhexose; HexNAc, *N*-acetylhexosamine.

Peak no. ESC	*m/z*	Composition
1	934.39	Hex_3
2	1096.44	Hex_4
3	1137.47	$Hex_3(HexNAc)_1$
4	1178.50	$Hex_2(HexNAc)_2$
5	1258.49	Hex_5
6	1299.52	$Hex_4(HexNAc)_1$
7	1324.55	$Hex_2(HexNAc)_2dHex_1$
8	1340.55	$Hex_3(HexNAc)_2$
9	1420.55	Hex_6
10	1461.57	$Hex_5(HexNAc)_1$
11	1486.61	$Hex_3(HexNAc)_2dHex_1$
12	1502.60	$Hex_4(HexNAc)_2$
13	1543.63	$Hex_3(HexNAc)_3$
14	1582.60	Hex_7
15	1623.63	$Hex_6(HexNAc)_1$
16	1645.66	$Hex_2(HexNAc)_2dHex_1$
17	1664.65	$Hex_5(HexNAc)_2$
18	1689.69	$Hex_3(HexNAc)_3dHex_1$
19	1705.68	$Hex_4(HexNAc)_3$
20	1746.71	$Hex_3(HexNAc)_4$
21	1785.68	$Hex_7(HexNAc)_1$
22	1826.71	$Hex_6(HexNAc)_2$
23	1848.74	$Hex_3(HexNAc)_3(NeuAc)_1$
24	1851.74	$Hex_4(HexNAc)_3dHex_1$
25	1867.73	$Hex_5(HexNAc)_3$
26	1892.76	$Hex_3(HexNAc)_4dHex_1$
27	1908.76	$Hex_4(HexNAc)_4$
28	1947.73	$Hex_8(HexNAc)_1$
29	1949.79	$Hex_3(HexNAc)_5$
30	1988.76	$Hex_7(HexNAc)_2$
31	2010.79	$Hex_4(HexNAc)_3(NeuAc)_1$
32	2013.79	$Hex_5(HexNAc)_3dHex_1$
33	2029.79	$Hex_6(HexNAc)_3$
35	2054.82	$Hex_4(HexNAc)_4dHex_1$
36	2070.81	$Hex_5(HexNAc)_4$
37	2095.84	$Hex_3(HexNAc)_5dHex_1$
38	2111.84	$Hex_4(HexNAc)_5$
39	2150.81	$Hex_8(HexNAc)_2$
40	2156.85	$Hex_4(HexNAc)_3dHex_1(NeuAc)_1$
41	2172.84	$Hex_5(HexNAc)_3(NeuAc)_1$
42	2175.84	$Hex_6(HexNAc)_3dHex_1$
43	2191.84	$Hex_7(HexNAc)_3$
44	2200.88	$Hex_4(HexNAc)_4dHex_2$
45	2213.87	$Hex_4(HexNAc)_4(NeuAc)_1$
46	2216.87	$Hex_5(HexNAc)_4dHex_1$
47	2232.92	$Hex_6(HexNAc)_4$
48	2257.90	$Hex_4(HexNAc)_5dHex_1$
49	2273.90	$Hex_5(HexNAc)_5$
50	2298.92	$Hex_3(HexNAc)_6dHex_1$
51	2312.86	$Hex_9(HexNAc)_2$
52	2318.90	$Hex_5(HexNAc)_3dHex_1(NeuAc)_1$
53	2334.90	$Hex_6(HexNAc)_3(NeuAc)_1$
54	2359.93	$Hex_4(HexNAc)_4dHex_1(NeuAc)_1$
55	2375.92	$Hex_5(HexNAc)_4(NeuAc)_1$
56	2378.92	$Hex_6(HexNAc)_4dHex_1$
57	2394.92	$Hex_7(HexNAc)_4$
58	2403.95	$Hex_4(HexNAc)_5dHex_2$
59	2419.95	$Hex_5(HexNAc)_5dHex_1$
60	2460.98	$Hex_4(HexNAc)_6dHex_1$
61	2474.92	$Hex_{10}(HexNAc)_2$
62	2480.95	$Hex_6(HexNAc)_3dHex_1(NeuAc)_1$
63	2508.99	$Hex_5(HexNAc)_4dHex_3$
64	2521.98	$Hex_5(HexNAc)_4dHex_1(NeuAc)_1$
65	2537.98	$Hex_6(HexNAc)_4(NeuAc)_1$
66	2540.98	$Hex_7(HexNAc)_5dHex_1$
67	2566.01	$Hex_5(HexNAc)_5dHex_2$
68	2651.33	Internal standard
69	2668.04	$Hex_5(HexNAc)_4dHex_2(NeuAc)_1$
70	2681.03	$Hex_5(HexNAc)_4(NeuAc)_2$
71	2684.03	$Hex_6(HexNAc)_4dHex_1(NeuAc)_1$
72	2712.79	$Hex_5(HexNAc)_4(NeuGc)_2$
73	2827.09	$Hex_5(HexNAc)_4dHex_1(NeuAc)_2$

of individual culture conditions used on the ratio of these glycotypes must be examined carefully.

DISCUSSION

For most mammalian cell types, it is not known which proteins are expressed at each cellular stage and how these protein expression patterns change quantitatively upon differentiation and proliferation. Flow cytometry and immunohistochemistry have been generally used for the identification of cell surface proteins such as cell differentiation markers. However, it is not currently possible to profile a global view of the cell surface protein landscape due to the limitation of feasible antibodies with validated specificity and affinity strength and the difficulty in the development of multiplexed assays for identifying sets of cell surface proteins in a single experiment.

Large scale proteomics analysis by two-dimensional gel electrophoresis MALDI-TOF-MS suggested that only 17 proteins (0.7% of total detected ~2200 proteins) with different expression patterns may be involved in the DMSO-induced cardiac differentiation of P19CL6 cells (36). They also reported that real time PCR data showed discrepancies from that of proteomics in at least three kinds of proteins that reflected the importance of posttranslational modifications in expressed proteins. On the other hand, it was also reported that only 0.8% of total detected proteins (28 proteins of ~3500 proteins) were increased or decreased during the 8-day differentiation of P19 cells to neural cells (34, 37). Consequently, it was concluded that changes in the expression level of detected proteins are not helpful for identifying or monitoring the processes of cellular differentiation of both P19 and P19C6 cells. Compared with the results of proteome-based analysis, the high potential of the glycome-based approach is clear because our results revealed for the first time that 28% of glycoforms (19 *N*-glycans of 67 total *N*-glycans; peak numbers 13, 20, 21, 22, 25, 28, 29, 32, 34, 37, 38, 39, 40, 41, 47, 48, 54, 60, and 63) were increased, and 10% (7 of 67) were decreased during P19CL6 cell differentiation to car-

diomyocytes. Furthermore, the expression level of 31 *N*-glycans involved in the glycotype MF was up-regulated to 34% (78.2 pmol/200 μg of protein) against total detected *N*-glycan expression (239.5 pmol/200 μg of protein), whereas undifferentiated cells expressed only 15% glycotype MF (20 glycoforms). Interestingly, differentiated cardiomyocytes lost most Lewis X trisaccharide (SSEA-1) and sialyl-Lewis X tetrasaccharide moieties in major *N*-glycans as shown in Fig. 3*C*, whereas monofucosylation occurred specifically in the above 31 glycoforms at the GlcNAc residue involved in core chitobiose moiety after differentiation, suggesting that loss of cell adhesion through the interaction with selectins may be key to the differentiation of P19CL6 cells toward cardiomyocytes. It was also demonstrated that both P19C6 cells and ESCs showed quite similar drastic changes in the profiles of entire *N*-glycan expression during cell differentiation into neural cells in which the expression level of glycotype BS was up-regulated to 12 and 14% from 3 and 5%, respectively. Among *N*-glycans involved in the glycotype BS, three common bisect type glycoforms detected in neural cells were found to become new potential markers to identify and monitor the process of mouse neural cell differentiation. Given that the glycoforms corresponding to these three bisect type *N*-glycans have been known to exist in the mouse brain system (38, 39), this drastic up-regulation of the *N*-glycans involved in glycotype BS seems to be crucial for the differentiation to neural cells. Actually, GlcNAc-transferase III (*Mgat3* gene), a glycosyltransferase responsible for the synthesis of bisecting GlcNAc linkage, appears to be normally expressed at high levels in mammalian brain and kidney tissues (40, 41). However, the relationship between threshold in the expression level of glycotype BS and mechanism in P19C6 cell differentiation remains unclear.

In the present study, we demonstrated the versatility of glycoblotting-based quantitative glycomics in the investigation of dynamic glycoform alteration during mammalian cell proliferation and differentiation. A full portrait of *N*-glycan expression at each cell stage allowed identification of the characteristic glycotypes showing drastic and concerted expression changes during cell differentiation, termed stage-specific embryonic glycotypes. The present results indicate the existence of a threshold in expression level of the characteristic glycotypes required for initiating individual cell differentiations, although functional roles, mechanism, and designated partner molecules remain unknown. A microarray displaying major glycotypes expressed at individual cell stages should be a useful tool to elicit candidate partner molecules as well as the adhesion mechanism of the differentiated cells. However, we consider that most glycoproteins at the specific cell stage might share some biosynthetic pathways at the Golgi, resulting in the dynamic and large scale expression changes of glycotypes during cell differentiation. We should set a goal to compare and accumulate a database of whole *N*-glycan expression levels of feasible human ESC and iPS cell lines established by different laboratories and to make these resources readily available to the scientific community as soon as possible.

* This work was supported in part by a grant for "Innovative program for future drug discovery and medical care" from the Japan Science and Technology Agency and the Ministry of Education, Culture, Science, Sports, and Technology of Japan.

‖ To whom correspondence should be addressed. E-mail: shin@glyco.sci.hokudai.ac.jp.

REFERENCES

1. Stanton, L. W., and Bakre, M. M. (2007) Genomic and proteomic characterization of embryonic stem cells. *Curr. Opin. Chem. Biol.* **11,** 399–404
2. Kuramitsu, Y., and Nakamura, K. (2006) Proteomic analysis of cancer tissues: shedding light on carcinogenesis and possible biomarkers. *Proteomics* **6,** 5650–5661
3. Gonnet, F., Bouazza, B., Millot, G. A., Ziaei, S., Garcia, L., Butler-Browne, G. S., Mouly, V., Tortajada, J., Danos, O., and Svinartchouk, F. (2008) Proteome analysis of differentiating human myoblasts by dialysis-assisted two-dimensional gel electrophoresis (DAGE). *Proteomics* **8,** 264–278
4. Watkins, J., Basu, S., and Bogenhagen, D. F. (2008) A quantitative proteomic analysis of mitochondrial participation in p19 cell neuronal differentiation. *J. Proteome Res.* **7,** 328–338
5. Loring, J. F., and Rao, M. S. (2006) Establishing standards for the characterization of human embryonic stem cell lines. *Stem Cells* **24,** 145–150
6. Varki, A. (1993) Biological roles of oligosaccharides: all of the theories are correct. *Glycobiology* **3,** 97–130
7. Haltiwanger, R. S., and Lowe, J. B. (2004) Role of glycosylation in development. *Annu. Rev. Biochem.* **73,** 491–537
8. Guérardel, Y., Chang, L. Y., Maes, E., Huang, C. J., and Khoo, K. H. (2006) Glycomic survey mapping of zebrafish identifies unique sialylation pattern. *Glycobiology* **16,** 244–257
9. Ohtsubo, K., and Marth, J. D. (2006) Glycosylation in cellular mechanisms of health and disease. *Cell* **126,** 855–867
10. Solter, D., and Knowles, B. B. (1978) Monoclonal antibody defining a stage-specific mouse embryonic antigen (SSEA-1). *Proc. Natl. Acad. Sci. U.S.A.* **75,** 5565–5569
11. Kannagi, R., Cochran, N. A., Ishigami, F., Hakomori, S., Andrews, P. W., Knowles, B. B., and Solter, D. (1983) Stage-specific embryonic antigens (SSEA-3 and -4) are epitopes of a unique globo-series ganglioside isolated from human teratocarcinoma cells. *EMBO J.* **2,** 2355–2361
12. Lau, K. S., Partridge, E. A., Grigorian, A., Silvescu, C. I., Reinhold, V. N., Demetriou, M., and Dennis, J. W. (2007) Complex *N*-glycan number and degree of branching cooperate to regulate cell proliferation and differentiation. *Cell* **129,** 123–134
13. Lanctot, P. M., Gage, F. H., and Varki, A. P. (2007) The glycans of stem cells. *Curr. Opin. Chem. Biol.* **11,** 373–380
14. Surani, M. A. (1979) Glycoprotein synthesis and inhibition of glycosylation by tunicamycin in preimplantation mouse embryos: compaction and trophoblast adhesion. *Cell* **18,** 217–227
15. Akama, T. O., Nakagawa, H., Sugihara, K., Narisawa, S., Ohyama, C., Nishimura, S., O'Brien, D. A., Moremen, K. W., Millan, J. L., and Fukuda, M. N. (2002) Germ cell survival through carbohydrate-mediated interaction with Sertoli cells. *Science* **295,** 124–127
16. Shur, B. D., Rodeheffer, C., and Ensslin, M. A. (2004) Mammalian fertilization. *Curr. Biol.* **14,** R691–R692
17. Hato, M., Nakagawa, H., Kurogochi, M., Akama, T. O., Marth, J. D., Fukuda, M. N., and Nishimura, S. I. (2006) Unusual *N*-glycan structures in alpha-mannosidase II/IIx double null embryos identified by a systematic glycomics approach based on two-dimensional LC mapping and matrix-dependent selective fragmentation method in MALDI-TOF/TOF mass spectrometry. *Mol. Cell. Proteomics* **5,** 2146–2157
18. Eggens, I., Fenderson, B., Toyokuni, T., Dean, B., Stroud, M., and Hakomori, S. (1989) Specific interaction between Le^x and Le^x determinants. *J. Biol. Chem.* **264,** 9476–9484
19. Muramatsu, T., and Muramatsu, H. (2004) Carbohydrate antigens expressed on stem cells and early embryonic cells. *Glycoconj. J.* **21,** 41–45
20. Varki, A. (2007) Glycan-based interactions involving vertebrate sialic acid-

recognizing proteins. *Nature* **446,** 1023–1029
21. Martin, M. J., Muotri, A., Gage, F., and Varki, A. P. (2005) Human embryonic stem cells express an immunogenic nonhuman sialic acid. *Nat. Med.* **11,** 228–232
22. Takahashi, K., Tanabe, K., Ohnuki, M., Narita, M., Ichisaka, T., Tomoda, K., and Yamanaka, S. (2007) Induction of pluripotent stem cells from adult human fibroblasts by defined factors. *Cell* **131,** 861–872
23. Sakurada, K., McDonald, F. M., and Shimada, F. (2008) Regenerative medicine and stem cell based drug discovery. *Angew. Chem. Int. Ed. Engl.* **47,** 5718–5738
24. Pilobello, K. T., and Mahal, L. K. (2007) Deciphering the glycocode: the complexity and analytical challenge of glycomics. *Curr. Opin. Chem. Biol.* **11,** 300–305
25. Nishimura, S., Niikura, K., Kurogochi, M., Matsushita, T., Fumoto, M., Hinou, H., Kamitani, R., Nakagawa, H., Deguchi, K., Miura, N., Monde, K., and Kondo, H. (2004) High-throughput protein glycomics: combined use of chemoselective glycoblotting and MALDI-TOF/TOF mass spectrometry. *Angew. Chem. Int. Ed. Engl.* **44,** 91–96
26. Furukawa, J., Shinohara, Y., Kuramoto, H., Miura, Y., Shimaoka, H., Kurogochi, M., Nakano, M., and Nishimura, S. I. (2008) Comprehensive approach to structural and functional glycomics based on chemoselective glycoblotting and sequential tag conversion. *Anal. Chem.* **80,** 1094–1101
27. Edwards, M. K., Harris, J. F., and McBurney, M. W. (1983) Induced muscle differentiation in an embryonal carcinoma cell line. *Mol. Cell. Biol.* **3,** 2280–2286
28. Stanley, P. (2002) Biological consequences of overexpressing or eliminating *N*-acetylglucosaminyltransferase-TIII in mouse. *Biochim. Biophys. Acta* **1573,** 363–368
29. Gao, X., Bian, W., Yang, J., Tang, K., Kitani, H., Atsumi, T., and Jing, N. A. (2001) role of *N*-cadherin in neuronal differentiation of embryonic carcinoma P19 cells. *Biochem. Biophys. Res. Commun.* **284,** 1098–1103
30. Tang, K., Yang, J., Gao, X., Wang, C., Liu, L., Kitani, H., Atsumi, T., and Jing, N. (2002) Wnt-1 promotes neuronal differentiation and inhibits gliogenesis in P19 cells. *Biochem. Biophys. Res. Commun.* **293,** 167–173
31. Yagi, T., Tokunaga, T., Furuta, Y., Nada, S., Yoshida, M., Tsukada, T., Saga, Y., Takeda, N., Ikawa, Y., and Aizawa, S. (1993) A novel ES cell line, TT2, with high germ line-differentiating potency. *Anal. Biochem.* **214,** 70–76
32. Miura, Y., Hato, M., Shinohara, Y., Kuramoto, H., Furukawa, J., Kurogochi, M., Shimaoka, H., Tada, M., Nakanishi, K., Ozaki, M., Todo, S., and Nishimura, S. I. (2008) BlotGlycoABC™, an integrated glycoblotting technique for rapid and large scale clinical glycomics. *Mol. Cell. Proteomics* **7,** 370–377
33. McBurney, M. W., Jones-Villeneuve, E. M., Edwards, M. K., and Anderson, P. J. (1982) Control of muscle and neuronal differentiation in a cultured embryonal carcinoma cell line. *Nature* **299,** 165–167
34. Habara-Ohkubo, A. (1996) Differentiation of beating cardiac muscle cells from a derivative of P19 embryonal carcinoma cells. *Cell Struct. Funct.* **21,** 101–110
35. Inberg, A., Bogoch, Y., Bledi, Y., and Linial, M. (2007) Cellular processes underlying maturation of P19 neurons: changes in protein folding regimen and cytoskeleton organization. *Proteomics* **7,** 910–920
36. Baharvand, H., Piryaei, A., Rohani, R., Taei, A., Heidari, M. H., and Hosseini, A. (2006) Ultrastructural comparison of developing mouse embryonic stem cell- and *in vivo*-derived cardiomyocytes. *Cell Biol. Int.* **30,** 800–807
37. Wen, J., Xia, Q., Lu, C., Yin, L., Hu, J., Gong, Y., Yin, B., Monzen, K., Yuan, J., Qiang, B., Zhang, X., and Peng, X. (2007) Proteomic analysis of cardiomyocytes differentiation in mouse embryonic carcinoma P19CL6 cells. *J. Cell. Biochem.* **102,** 149–160
38. An, J., Yuan, Q., Wang, C., Liu, L., Tang, K., Tian, H. Y., Jing, N. H., and Zhao, F. K. (2005) Differential display of proteins involved in the neural differentiation of mouse embryonic carcinoma P19 cells by comparative proteomic analysis. *Proteomics* **5,** 1656–1668
39. Zamze, S., Harvey, D. J., Pesheva, P., Mattu, T. S., Schachner, M., Dwek, R. A., and Wing, D. R. (1999) Glycosylation of a CNS-specific extracellular matrix glycoprotein, tenascin-R, is dominated by O-linked sialylated glycans and "brain-type" neutral *N*-glycans. *Glycobiology* **9,** 823–831
40. Shimizu, H., Ochiai, K., Ikenaka, K., Mikoshiba, K., and Hase, S. (1993) Structures of *N*-linked sugar chains expressed mainly in mouse brain. *J. Biochem.* **114,** 334–338
41. Priatel, J. J., Sarkar, M., Schachter, H., and Marth, J. D. (1997) Isolation, characterization and inactivation of the mouse *Mgat3* gene: the bisecting *N*-acetylglucosamine in asparagines-linked oligosaccharides appears dispensable for viability and reproduction. *Glycobiology* **7,** 45–56

Osteoarthritis and Cartilage 18 (2010) 1133–1143

Osteoarthritis and Cartilage

Changes of human menisci in osteoarthritic knee joints

Y. Katsuragawa †‡, K. Saitoh †‡[a], N. Tanaka §, M. Wake §, Y. Ikeda §, H. Furukawa §, S. Tohma §, M. Sawabe ||, M. Ishiyama ¶, S. Yagishita ¶, R. Suzuki §, H. Mitomi #, N. Fukui §*

† *Department of Orthopaedic Surgery, National Center for Global Health and Medicine, Tokyo, Japan*
‡ *Department of Pathology, National Center for Global Health and Medicine, Tokyo, Japan*
§ *Clinical Research Center, National Hospital Organization, Sagamihara Hospital, Kanagawa, Japan*
|| *Department of Pathology, Tokyo Metropolitan Geriatric Hospital, Tokyo, Japan*
¶ *Department of Clinical Laboratory, Kanagawa Rehabilitation Hospital, Kanagawa, Japan*
# *Department of Pathology, Jyuntendo University School of Medicine, Tokyo, Japan*

ARTICLE INFO

Article history:
Received 16 November 2009
Accepted 29 May 2010

Keywords:
Osteoarthritis
Meniscus
IGF-1 (insulin-like growth factor-1)

SUMMARY

Objective: To investigate the changes of knee menisci in osteoarthritis (OA) in human.
Methods: OA and control menisci were obtained from 42 end-stage OA knees with medial involvement and 28 non-arthritic knees of age-matched donors, respectively. The change of menisci in OA was evaluated by histology, and gene expression of major matrix components and anabolic factors was analyzed in the anterior horn segments by quantitative PCR (qPCR). In those regions of menisci, the rate of collagen neo-synthesis was evaluated by [^{3}H]proline incorporation, and the change of matrix was investigated by ultrastructural observation and biomechanical measurement.
Results: In OA menisci, the change in histology was rather moderate in the anterior horn segments. However, despite the modest change in histology, the expression of type I, II, III procollagens was dramatically increased in those regions. The expression of insulin-like growth factor 1 (IGF-1) was markedly enhanced in OA menisci, which was considered to be responsible, at least partly, for the increase in procollagen gene expression. Interestingly, in spite of marked increase in procollagen gene expression, incorporation of [^{3}H]proline increased only modestly in OA menisci, and impaired collagen synthesis was suggested. This finding was consistent with the results of ultrastructural observation and biomechanical measurement, which indicated that the change of meniscal matrix was modest in the macroscopically preserved areas of OA menisci.
Conclusion: Although the expression of major matrix components was markedly enhanced, matrix synthesis was enhanced only modestly, and the changes of matrix in human OA menisci were rather modest in the non-degenerated areas.

Introduction

With the increasing human life expectancy, osteoarthritis (OA) has now become a leading cause of disability among older adults[1]. A knee joint is one of the most susceptible joints to OA, and OA of the knees accounts for a large part of the OA-related disability. In OA knees, almost all joint structures are affected by the disease. Knee menisci are also known to undergo an obvious change in OA[2].

Menisci are C-shaped fibrocartilaginous structures that are predominantly composed of type I, with small amounts of type II, type III collagens and proteoglycans[3–11]. Located between the femoral condyles and tibial plateau, menisci play important roles in load transmission, shock absorption, and maintenance of joint stability[12]. With the progression of OA, menisci undergo degenerative changes such as wearing and laceration[2]. Subluxation of menisci also occurs[13]. Reflecting their functional importance, the changes in menisci are closely associated with the initiation and progression of OA[14,15]. Although often studied in animal models, human OA menisci have seldom been the subject of investigation, and it is still not known well how menisci change in OA.

A meniscus is not a homogeneous tissue. Regional differences in tissue composition and cell metabolism have been observed between the inner and outer areas, and structural differences have been noticed between the surface and central regions[4,8–11,16–19]. Therefore, the evaluation of meniscus pathology would be more reasonably performed if such regional differences were considered.

* Address correspondence and reprint requests to: Naoshi Fukui, Clinical Research Center, National Hospital Organization, Sagamihara Hospital, Sakuradai 18-1, Sagamihara, Minami-ku, Kanagawa 252-0315, Japan. Tel/Fax: 81-42-742-8311.
E-mail address: n-fukui@sagamihara-hosp.gr.jp (N. Fukui).
[a] Deceased.

1063-4584/$ – see front matter © 2010 Osteoarthritis Research Society International. Published by Elsevier Ltd. All rights reserved.
doi:10.1016/j.joca.2010.05.017

In this study, human menisci from OA and control knees were investigated by histological and molecular biological analyses, paying special attention to the regional differences within menisci. The rate of collagen neosynthesis was determined, and the change of meniscal matrix was evaluated by ultrastructural analysis and biomechanical measurement. The results of these analyses revealed the unique nature of the changes in human OA menisci, which are considerably different from those reported in animal studies.

Materials and methods

Material collection

This study was performed with the approval of the Human Ethics Review Committees of the participating institutions, and informed consent was obtained in writing from each subject or family of the donor before material collection. OA menisci were obtained in pairs of lateral and medial menisci from 42 OA knee joints of 40 patients within 4 h after a prosthetic surgery. The diagnosis of OA was based on the criteria of the American College of Rheumatology for OA[20], and all knee joints were medially involved in the disease. Control menisci were obtained from 28 non-arthritic knee joints of 22 donors (obtained bilaterally in six donors; ages 73–92 with a mean of 84) within 24 h after death. The donors were chosen from those who did not have a past record of treatment for joint disease or trauma, and the normality of the joint was confirmed macroscopically at the time of sample harvest. Prior to the analyses, all OA and control menisci were photographed and their macroscopic appearance was recorded. Control menisci were inspected closely, and were not used for the study if they showed overt signs of macroscopic degeneration. In this study, evaluations were performed on the anterior horn segments of menisci unless specified otherwise. This was because that those segments were well preserved in OA menisci, which made it possible to compare the changes in OA menisci directly in a site-to-site manner with those in the control menisci. Posterior horn segments of menisci were also often preserved in OA knees, but those segments were not used for the analyses. In this work, the OA and control menisci were randomly assigned to respective analyses. Some menisci were used for two or more evaluations.

Histological evaluation

Ten pairs of OA menisci and eight pairs of control menisci were used for this evaluation. The evaluation was performed primarily on the anterior horn segments of menisci, but for OA medial menisci, the body sections were also observed in order to know the changes in degenerated regions. Meniscus tissues were fixed in 4% paraformaldehyde, and 4-μm-thick sections were prepared in a plane perpendicular to the surface. The sections were stained with hematoxylin and eosin or Masson's trichrome stain, and observed under a light microscope. For the immunodetection of insulin-like growth factor (IGF)-1, the sections were pretreated with proteinase K (DakoCytomation, Carpinteria, California) and then incubated with a monoclonal antibody for human IGF-1 (Millipore, Billerica, Massachusetts). The primary antibody was reacted with the secondary antibody conjugated with streptavidine, which was visualized with 3,3′-diaminobenzidine (DAB), tetrahydrochloride using a commercially available kit (ChemMate EnVision Detection, DakoCytomation). The nuclei were stained with hematoxylin, and the localization of staining was observed under a light microscope.

Gene expression analysis

Twelve pairs of OA and control menisci were used for the evaluation. For the analysis, meniscus tissues were obtained from the anterior horn segments with a width of approximately 5 mm (Fig. 1). Immediately after harvest, the tissue was divided into four regions under a dissection microscope (Fig. 2). The divided tissues were each embedded in OCT compound (Sakura Finetechnical, Tokyo, Japan), snap frozen in liquid nitrogen, and stored at −80 °C until use. RNA was extracted from each of these regions by a previously described method[21]. cDNA was synthesized using the Sensiscript reverse transcriptase (Qiagen, Hilden, Germany) with a routine use of DNase I (Qiagen). Gene-specific primers and probes were prepared (Table I), and quantitative PCR (qPCR) was performed using either SYBR Premix Ex Taq or Premix Ex Taq (both from Takara Bio, Shiga, Japan) on a LightCycler (Roche Diagnostics, Basel, Switzerland). The expression levels were normalized by the expression of glyceraldehyde-3-phosphate dehydrogenase (*GAPDH*). For some samples, β-actin (*ACTB*) expression was also used for normalization.

Evaluation of collagen neosynthesis

The rate of collagen biosynthesis was determined by quantifying the amount of [^{3}H]proline incorporation into meniscus explants. Eight pairs of OA menisci and six pairs of control menisci were used for this analysis. The explants were prepared from the anterior horn segments of those menisci. In each of these menisci, the anterior horn segment was separated from the body segment, and the entire part of that segment was cut into 1–2 mm cubes, or explants. Four to six explants were placed in each of the 24-well tissue culture plates, which were maintained in Dulbecco's modified eagle medium (DMEM) containing 10% fetal bovine serum (FBS) and 25 μg/ml ascorbic acid. Forty-eight hours later, the media were then replaced by those containing 0.1% FBS, 25 μg/ml ascorbic acid and 10 μCi/ml [^{3}H]proline. After 8 h, the media were removed and the

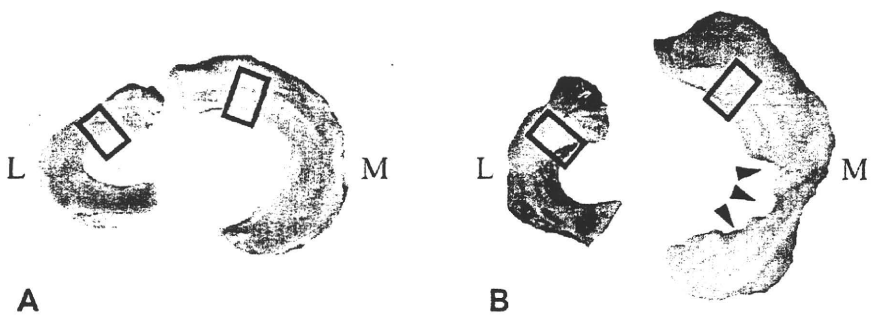

Fig. 1. Gross appearance of control and OA menisci. Representative photographs of control (A) and OA menisci (B) are shown. In each meniscus, a pair of parallel lines indicates the region in the anterior horn segment used for molecular biological analysis. In B, arrowheads indicate degenerated area in medial meniscus. M and L indicate medial and lateral menisci, respectively.

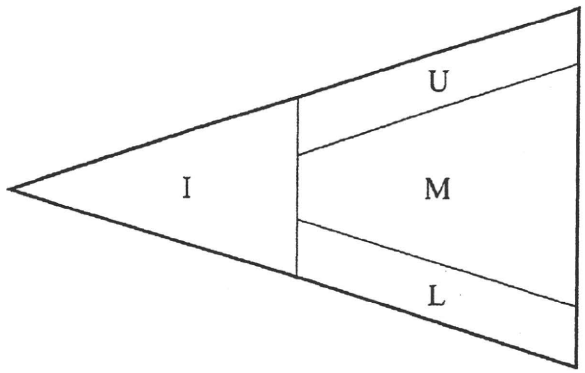

Fig. 2. Separation of meniscus regions. Anterior horn segment of meniscus was divided into inner (I), and outer halves, and the latter was further divided into upper surface (U), middle (M), and lower surface (L) regions. Gene expression was evaluated in those regions respectively. Cross-section of a meniscus is shown.

explants were rinsed three times with ice-cold phosphate-buffered saline (PBS). The samples were stored at −20 °C until use.

To determine the rate of [^{3}H]proline incorporation, the explants were minced and digested with proteinase K (2 mg/ml; Sigma, St. Louis, Missouri) at 58 °C for 48 h. After digestion, the samples were centrifuged and radioactivity of the supernatant was measured. The radioactivity was normalized by DNA content, which was determined by Quant-iT PicoGreen dsDNA assay kit (Invitrogen, Carlsbad, California).

Transmission electron microscopy

Three pairs of OA menisci and three pairs of control menisci were used for the evaluation. For the analysis, the tissues were obtained as thin slices from the anterior horn segments, which were immediately immersed in 2.5% glutalaldehyde in the cacodylate buffer. The samples were then treated with 1% OsO_4 in cacodylate buffer, dehydrated in graded concentration of ethanol, and embedded in epon with careful attention to the orientation. Sections were cut at 90 nm thickness and stained sequentially with 0.2% oolong tea extract (Nisshin EM, Tokyo, Japan), aqueous uranyl acetate, and lead citrate. The sections were observed under a JOEL JEM-2000 FX-II electron microscope (Nihon Denshi, Tokyo, Japan).

Quantitative image analysis of collagen fibrils was performed following a previously described method[22] with some modifications. In brief, three to five photomicrographs were taken on each section at the magnification of ×20,000, and on each photo, the number and diameters of collagen fibrils were determined using an image analysis software (ImageJ version 1.42e; National Institute of Health, Bethesda, Maryland). For each meniscus, mean fibril diameter, number of fibrils per μm^2, and percentage of the area occupied by fibrils were determined.

Table I
Primer and probe sequences used for quantitative PCR

Gene	Primer and probe sequence	T_m
COL1A1	Forward: 5′-AGCCTGGGGCAAGACAGTGATT-3′ Reverse: 5′-TTGCTTGTCTGTTTCCGGGTTG-3′	60
COL1A2	Forward: 5′-ATGAGGAGACTGGCAACCTGAAAAA-3′ Reverse: 5′-TCCAAAGGTGCAATATCAAGGAAGG-3′	58
COL2A1	Forward: 5′-GACATAGGAGGGCCCGAGCA-3′ Reverse: 5′-CGGCACCTGAAGGGAGGTCT-3′	60
COL3A1	Forward: 5′-TCGAACACGCAAGGCTGTGAG-3′ Reverse: 5′-TGTCGGTCACTTGCACTGGTTGA-3′	60
ACAN	Forward: 5′-GCACGAGAAGGGCGAGTGGA-3′ Reverse: 5′-GCTCCTGGGCTCAGCGTCCT-3′	60
*IGF1**	Forward: 5′-GTACTTCAGAAGCAATGGGAAA-3′ Reverse: 5′-GTTGAAATAAAAGCCCCTGTCT-3′ Probe Flu: 5′-GTGAAGATGCACACCATGTCCTCCTCG-3′ LC: 5′-ATCTCTTCTACCTGGCGCTGTGCCTGC-3′	56
PDGFA	Forward: 5′-TCATTTACGAGATTCCTCGG-3′ Reverse: 5′-TGCTCCTCTAACCTCACCTG-3′	58
PDGFB	Forward: 5′-GGAAGAAGCCAATCTTTAAGAAG-3′ Reverse: 5′-CTTCAGTGCCGTCTTGTCAT-3′	58
TGFB1	Forward: 5′-ATGTTCTTCAACACATCAGAGC-3′ Reverse: 5′-GGTGACATCAAAAGATAACCAC-3′	58
GAPDH	Forward: 5′-AAAACCTGCCAAATATGATGAC-3′ Reverse: 5′-CAGGAAATGAGCTTGACAAAGT-3′	58
ACTB	Forward: 5′-ATTAAGGAGAAGCTGTGCTACGTC-3′ Reverse: 5′-ATGATGGAGTTGAAGGTAGTTTCG-3′	58

COL1A1, collagen, type I, alpha 1; *COL1A2*, collagen, type I, alpha 2; *COL2A1*, collagen, type II, alpha 1; *COL3A1*, collagen, type III, alpha 1; *ACAN*, aggrecan; *IGF1*, insulin-like growth factor 1; *PDGFA*, platelet-derived growth factor alpha polypeptide; *PDGFB*, platelet-derived growth factor beta polypeptide; *TGFB1*, transforming growth factor, beta1; *GAPDH*, glyceraldehyde-3-phsophate dehydrogenase; *ACTB*, actin, beta.

* Hybridization probes were used for quantitative PCR. Flu: probe conjugated with Fluorescein; LC: probe conjugated with LC640.

Biomechanical measurement

Six pairs of lateral and medial OA menisci and six pairs of control menisci were used for this analysis. For measurement, two to four cylindrical specimens, 4 mm in diameter, were harvested from the anterior horn segment of each meniscus. Those specimens were acquired along the periphery of the menisci, 1–2 mm inside from the outer margin, in a side-by-side manner. The number of obtained specimens varied among the menisci depending on the size and the severity of degeneration (when present). The specimens were prepared perpendicular to the tibial (lower) surface using a core reamer. After the acquisition, the upper part of the specimen was cut parallel to the tibial surface so that it would be 3 mm in height. Prior to the measurement, a wet weight of the specimen was determined.

Uniaxial confined compression test was performed according to a previously described method[23]. Each specimen was placed with the tibial surface facing down into a 4.0 mm diameter × 30 mm deep well in an acrylic chamber upon a porous filter. The chamber was then immersed in physiological saline in a reservoir, and the measurement was performed while the specimen was submerged in the saline. Compression load was applied to the specimen by a compression testing machine (Model SV-201NA, Imada Seisakusyo, Aichi, Japan). For measurement, a 4.0-mm diameter stainless indenter was gently inserted into the well in the acrylic chamber onto the specimen, and a constant load of 2 g was applied initially for 15 min as preloading. The load was then suddenly increased to 10 g, and the linear displacement rate was measured at 12 time points between 1 and 5000 s after the increase of the load. The applied load was maintained at 10 g throughout the measurement, which was monitored continuously with a load cell (Model LC-050N, Imada Seisakusyo). Two parameters, aggregate modulus (solid component stiffness) and permeability (measure of fluid flow through the tissue), which characterize the viscoelastic nature of the meniscus, were calculated using a nonlinear least squares optimization algorithm incorporating linear biphasic theory[24]. After biomechanical evaluation, the specimen was completely dried in a vacuum dryer and the dry weight was determined. Water content of the specimen was defined as the percentage of the weight lost by drying relative to that of the wet weight. Aggregate modulus, permeability, and water content were compared between OA and control menisci.

Statistics

Statistical significance of the data was evaluated using analysis of variance (ANOVA), and Fischer's Protected Least Significant Difference (PLSD) was used as a post-hoc test when necessary. Two-tailed *P*-values less than 0.05 were considered significant.

Results

Macroscopic observation

In control menisci, the anatomical shape was well preserved in all samples [Fig. 1(A)]. They had smooth surfaces and did not show macroscopic signs of degeneration except for the presence of slight fraying of the inner margin of the medial meniscus of four samples. For OA menisci, macroscopic appearance differed obviously between lateral and medial menisci. Since all OA menisci were obtained from medially involved knees, medial menisci underwent overt degenerative changes, while lateral menisci preserved the anatomical shape with few signs of macroscopic degeneration [Fig. 1(B)]. The changes of the medial menisci were most notable in the body and posterior horn segments, where the matrix was lost or severely fibrillated. Even in such menisci, the anterior horn segment was preserved well, showing few signs of matrix loss or degeneration.

Histological evaluation

The hematoxylin and eosin stained sections of the control lateral menisci showed short, thick wedge-shaped sections with smooth surfaces [Fig. 3(A) and (B)]. The inner area was filled with densely packed fibril bundles, and the cells were located sparsely throughout the menisci. In OA lateral menisci, fibril bundles tended to be obscure in the upper and lower surface regions, but the bundle structure was well preserved in the inner area away from the surfaces [Fig. 3(C) and (D)]. The cell density was similar to that in the controls.

Sections from control medial menisci showed a thinner, wedge-shaped cross-section with smooth surfaces [Fig. 3(E) and (F)]. Within the menisci, fibril bundles were densely packed and regularly aligned, resembling that of control lateral menisci. Meniscus cells were located sparsely, and the cell density was similar throughout the section. In medial menisci, changes with OA were more obvious than those in lateral menisci. Sections of OA medial menisci tended to be thicker than the controls, and the fibril bundles were not clearly recognized in the surface regions [Fig. 3 (G) and (H)]. In those regions, cell clusters were occasionally found. Structural change was also noticed in the inner areas, where fibril bundles were coarsely and unevenly distributed. Despite these changes, again, the cell density in OA medial menisci was similar to that of the controls.

Obvious wearing and fraying of fibril bundles was seen in the degenerated areas of OA medial menisci [Fig. 3(I) and (J)]. Even in such severely degenerated regions, cell density did not differ much from that of the controls, and cell clusters were found only occasionally.

Evaluation of matrix gene expression

Next, the expression of mRNA for matrix molecules that constitute menisci was evaluated. For this analysis, menisci were divided into inner, upper surface, middle, and lower surface regions (Fig. 2), and mRNA expression was determined in respective regions.

Considering primary components of menisci[3–11], expression of five matrix genes (*COL1A1*, *COL1A2*, *COL2A1*, *COL3A1* and *ACAN*) was evaluated in this study. First, the expression of two genes encoding type I procollagen (*COL1A1* and *COL1A2*) was evaluated. In control menisci, these genes were expressed at similar low levels in both lateral and medial menisci [Fig. 4(A) and (B)]. In OA menisci, the expression of these genes was dramatically increased in all four regions. The increase was 9- to 52-fold depending on the regions. While the expression of *COL1A1* was equally enhanced in lateral and medial OA menisci [Fig. 4(A)], *COL1A2* expression tended to be more enhanced in medial OA menisci [Fig. 4(B)]. As a consequence, in OA medial menisci, the expression ratios between *COL1A2* and *COL1A1* were significantly higher than those of the control medial menisci [Fig. 4(C)].

The expression of type II procollagen (*COL2A1*) was also enhanced in OA menisci in all four regions [Fig. 4(D)], although the level of increase was lower than that for type I procollagen genes (3- to 19-fold vs 9- to 52-fold).

Among the five genes evaluated, type III procollagen (*COL3A1*) was the one whose expression was most enhanced in OA menisci [Fig. 4(E)]. The increase reached as high as 400-fold. Similar to *COL1A2*, the expression of *COL3A1* tended to be more promoted in medial OA menisci than in lateral OA menisci.

In contrast to *COL3A1*, the increase of aggrecan (*ACAN*) expression in OA menisci was the least among the five genes, which never exceeded 2-fold [Fig. 4(F)].

Because the increase of gene expression in OA menisci was so dramatic, we repeated gene expression analysis of several samples using *ACTB* as an internal control. The result of this analysis confirmed the validity of the above results based on *GAPDH* expression (data not shown).

Expression of possible anabolic factors in OA menisci

In order to elucidate the mechanism(s) for enhanced matrix gene expression in OA menisci, a preliminary experiment was performed to investigate the expression of growth factor genes which could enhance anabolic activity of meniscal fibroblasts. We compared the expression of IGF-1 (*IGF1*), platelet growth factor (PDGF)-A (*PDGFA*), PDGF-B (*PDGFB*), and transforming growth factor (TGF)-β1 (*TGFB1*) between OA and control menisci, and found that the expression of *IGF1*, *PDGFA* and *PDGFB* was increased in OA menisci, while that of *TGFB1* was reduced [Fig. 5(A)–(D)]. Among these three genes, the increase in expression was most obvious with *IGF1*, which reached as high as 50-fold increase. The expression of *IGF1* tended to be higher in medial OA menisci than in lateral OA menisci, though this difference was not statistically significant. The expression of IGF-1 by OA meniscal cells was confirmed at the protein level by immunohistochemistry [Fig. 5(E) and (F)].

Evaluation of collagen neosynthesis

We next evaluated the rate of collagen neosynthesis in OA and control menisci by incorporation of [^{3}H]proline into meniscal explants. Collagens are the primary components of menisci that account for more than 75% of their dry weight[25,26]. Thus, the amount of incorporated [^{3}H]proline should represent the synthetic activity of meniscal cells. In control menisci, incorporation rate of [^{3}H]proline was similar between lateral and medial menisci (Table II). In OA menisci, the incorporation was increased above the control levels. However, the level of increase was rather low compared with the marked increase of procollagen mRNA expression in OA menisci. Because of the limited level of increase and a large variation among the samples, the increase of proline incorporation in OA menisci did not reach the level of significance in either lateral or medial OA menisci.

Ultrastructural evaluation

In order to study the change of meniscal matrix in depth, collagen fibril ultrastructure was evaluated by transmission electron microscopy. This observation was performed on the meniscal tissues obtained from the middle regions of the anterior horn segments (Fig. 2).

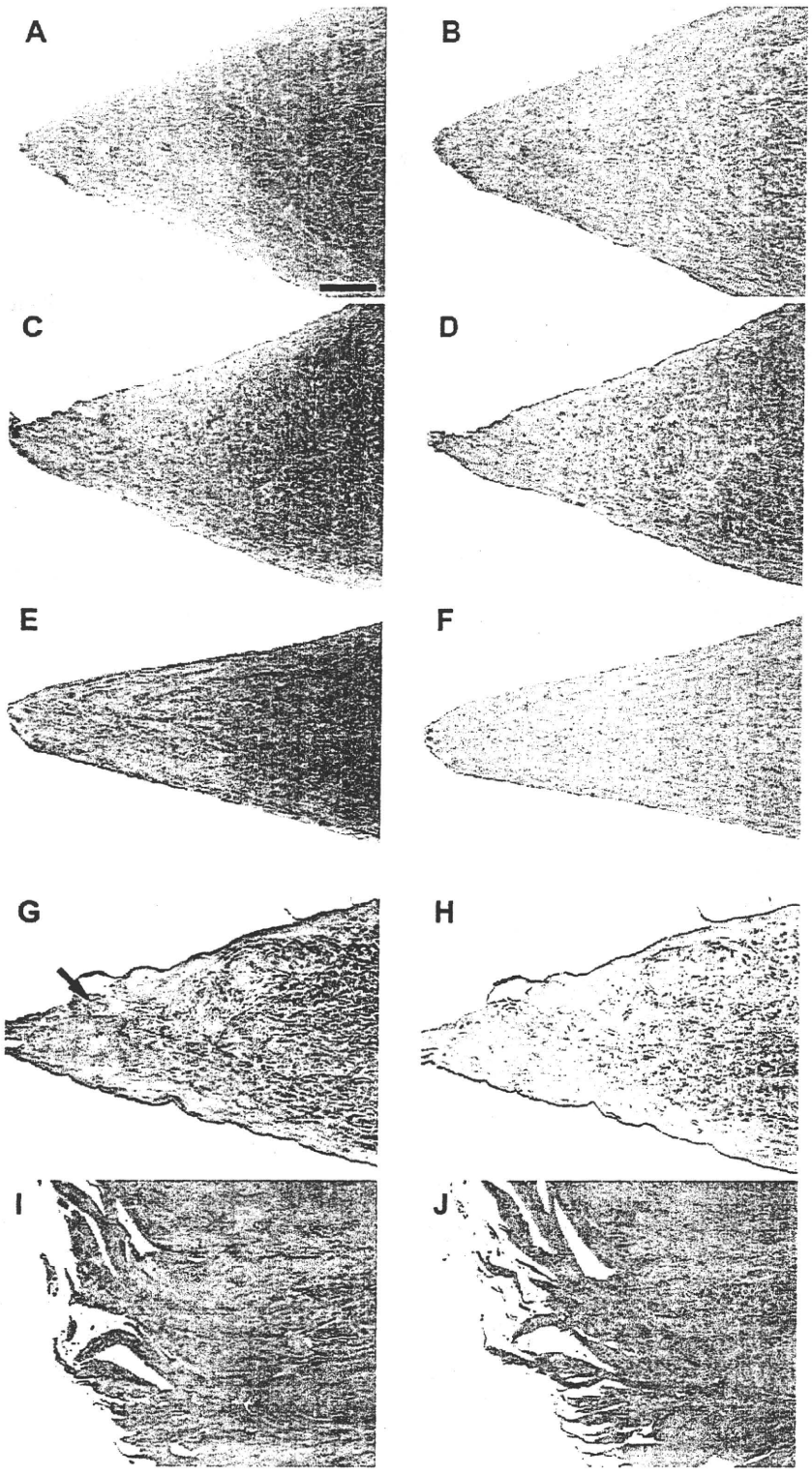

Fig. 3. Histology of OA and control menisci. Photomicrographs of sections from the anterior horn segments of control (A and B) and OA lateral menisci (C and D), and control (E and F) and OA medial menisci (G and H) are shown together with those from a degenerated area in the body segment of OA medial meniscus (I and J). In G, solid arrow indicates a cell cluster. Hematoxylin and eosin and Masson's trichrome stained sections are shown in left and right columns, respectively. Bar indicates 0.2 mm.

Consistent with previous reports[16,27], collagen fibrils in those regions were aligned in a circular orientation, and cross-sections of collagen fibrils were observed on the sections prepared perpendicular to the meniscus surfaces. Electron microscopy of control lateral menisci revealed that collagen fibrils of various diameters were densely packed in the matrix [Fig. 6(A)]. In OA lateral menisci, the change of collagen fibrils was rather modest, though fibrils of thinner diameters could have increased in

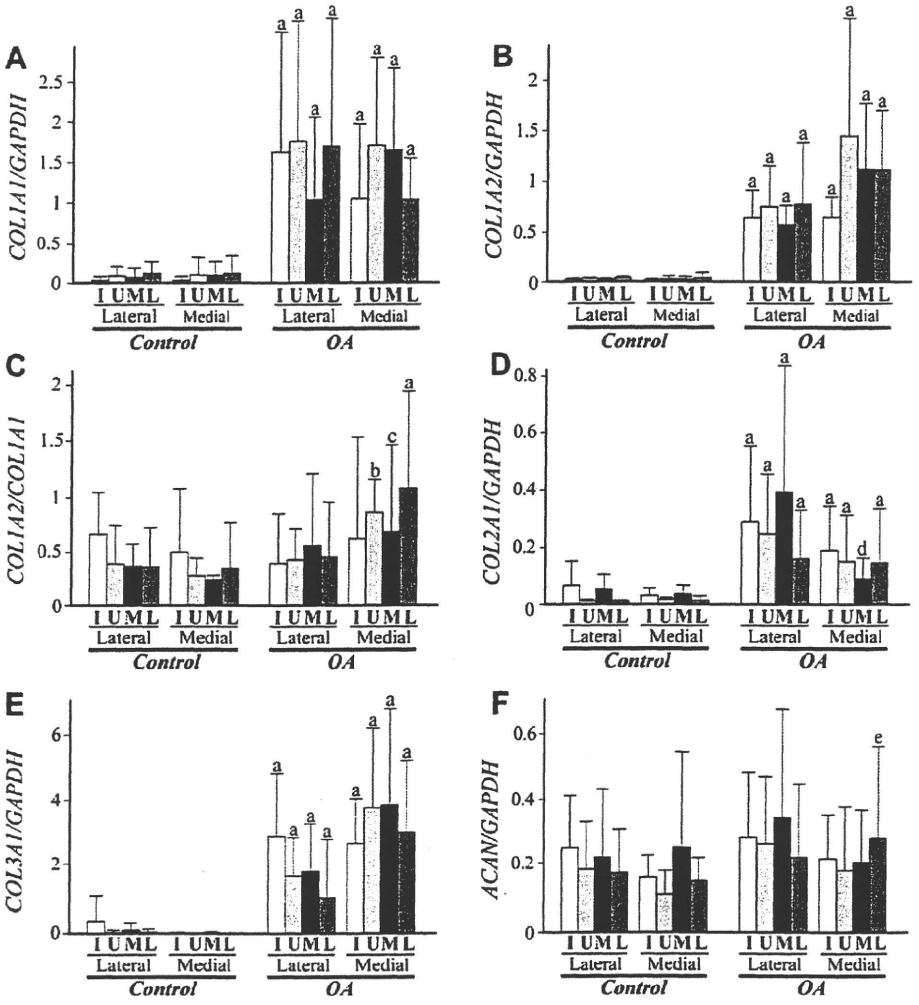

Fig. 4. Expression of matrix genes in OA and control menisci. Anterior horn segment of a meniscus was divided into four regions, and expression of matrix genes was evaluated in respective regions. Expression of type I (A and B), type II (D), type III (E) procollagen genes and aggrecan (F) is shown together with the expression ratio between two type I procollagen genes (C). In A, B, and D–F, results are shown by ratios against *GAPDH* expression. I, U, M, and L under bars indicate inner, upper surface, middle, and lower surface regions, respectively. Lateral and Medial indicate lateral and medial menisci, respectively. Results are shown by mean + 95% confidence interval. a, b, c, d and e indicate *P* values of <0.0001, 0.0092, 0.0021, 0.0086 and 0.0456, respectively, against corresponding region in control menisci.

number [Fig. 6(B)]. The change by OA was more obvious in medial menisci. Electron microscopy of the control medial menisci showed densely packed collagen fibrils with various diameters [Fig. 6(C)]. Although they resembled those of control lateral menisci, the fibrils tended to be more densely aligned. In OA medial menisci, the number of thinner fibrils increased obviously, and the fibrils were placed more sparsely [Fig. 6(D)]. The result of quantitative image analysis revealed that in OA medial menisci, the mean fibril diameter and percentage of the area occupied by fibrils were both significantly reduced, and the number of fibrils per area was significantly increased [Fig. 6(E)–(G)]. In lateral menisci, none of these parameters changed significantly by OA.

Biomechanical evaluation

Finally, the change in mechanical properties of meniscal matrix was evaluated by confined compression testing. Comparison of creep curves indicated that the mechanical properties could have changed by OA in medial menisci, while such changes might not be obvious in lateral menisci [Fig. 7(A)]. This was delineated by the changes in biomechanical parameters. Aggregate modulus of OA medial menisci was 40% lower than that of control medial menisci, whereas it differed little in lateral menisci [Fig. 7(B)]. In medial menisci, permeability changed more obviously. The permeability of OA medial menisci was more than 4-fold greater than that of the control medial menisci, while it changed little in lateral menisci [Fig. 7(C)]. Compared with these two parameters, the change of water content was modest. Although it tended to be higher in OA medial menisci, the increase was below the level of significance, and no significant change in this parameter was found between any two menisci [Fig. 7(D)].

Discussion

In this study, all OA menisci were obtained from OA knees with medial involvement, and the medial menisci were severely degenerated in the body segments. However, even in those menisci, the anterior horn segments were preserved well. This is why we performed most evaluations on the anterior horn segments, which made it possible to compare OA and control menisci in a site-to-site manner.

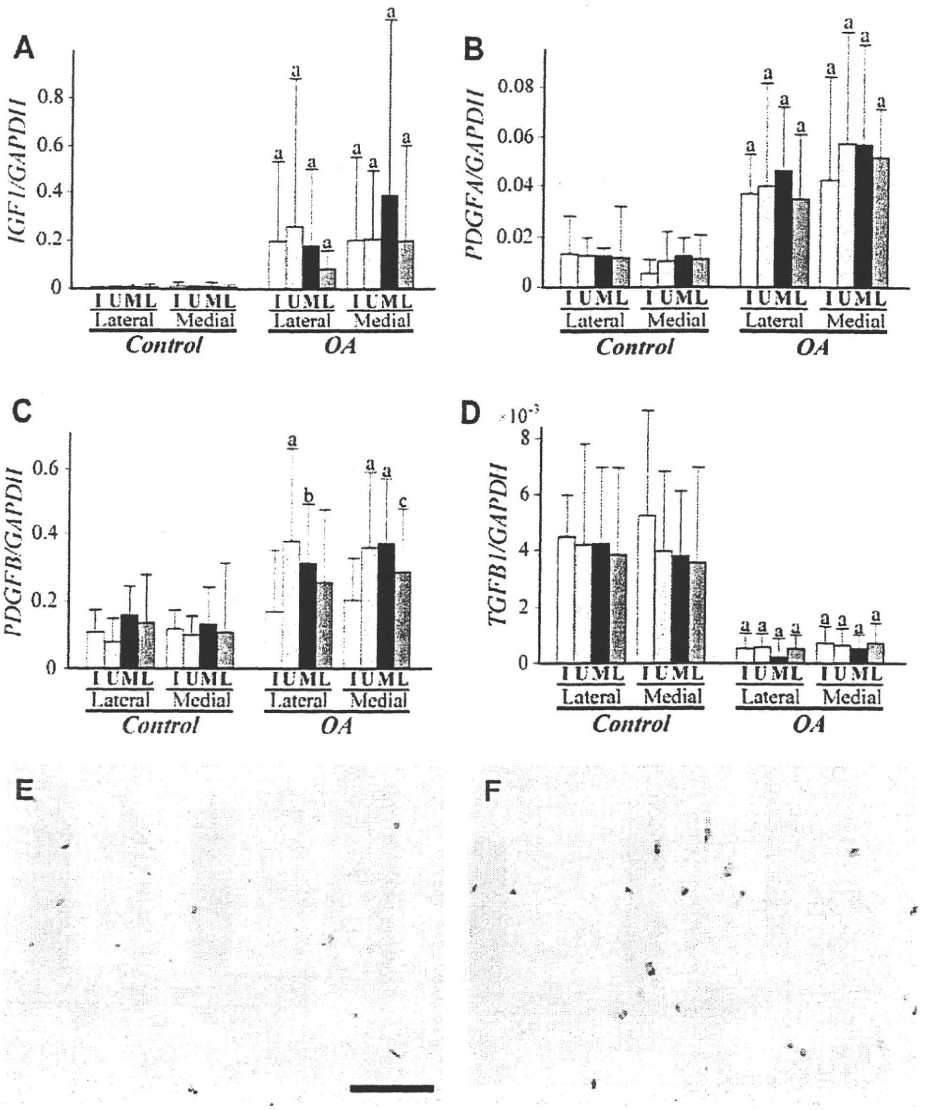

Fig. 5. Expression of possible anabolic factors in OA and control menisci. (A–D) Expression of *IGF1* (A), *PDGFA* (B), *PDGFB* (C) and *TGFB1* (D) in respective regions of OA and control menisci. Results are shown in the manner described for Fig. 4. a, b and c indicate *P* values of <0.0001, 0.0106 and 0.0028, respectively, against corresponding region in control menisci. (E and F) Immunohistochemistry for IGF-1. Photomicrographs of the sections from the middle regions of control (E) and OA menisci (F) are shown. Nuclei were stained with hematoxylin. Bar indicates 10 μm.

Consistent with the macroscopic appearance, the change in histology was moderate in the anterior horn segments of OA menisci. However, despite this limited change in histology, mRNA expression of major matrix components was markedly enhanced there. Among the five genes investigated, the increase in expression was most obvious with type I and type III procollagen, followed by type II procollagen, and least with aggrecan. This change in matrix gene expression could be the result of a reparative response that occurred within OA menisci. During the healing of fibrous tissues such as a ligament, tendon or skin, fibroblasts express type I and type III procollagens abundantly with the preponderance of type III procollagen[28,29]. We assume that this same mechanism could be involved in the enhancement of matrix gene expression in OA menisci. The result that the expression of type III procollagen tended to be more enhanced in the medial OA menisci than the lateral ones might suggest that such a reparative response could be more obvious in the medial compartment. This understanding seems reasonable since all OA knees studied here were medially involved in the disease.

Table II
[^{3}H]proline incorporation into meniscal explants

Meniscus		Scintillation count (cpm/μg DNA) (95% confidence interval)
Control	Lateral	3213 (0, 6963)
	Medial	3813 (1919, 5707)
OA	Lateral	7004 (0, 16,402)
	Medial	8345 (0, 20,875)

The result of qPCR analysis also revealed that the expression of IGF-1 was increased in OA menisci. Since IGF-1 has potent anabolic actions on meniscal cells[30–32], we consider that the increase in IGF-1 expression could be responsible for the enhanced matrix gene expression in OA menisci. In contrast to IGF-1, the expression of TGF-β1 was found to be reduced in OA menisci. This reduction in TGF-β1 expression could have a significant contribution to the degeneration of meniscal matrix. Besides the anabolic actions, TGF-β1